

TU

Dekanat der Fakultät für Maschinenbau

An den
Studiendekan
der Fakultät für Maschinenbau

Meldung über den Abschluß einer Diplomarbeit

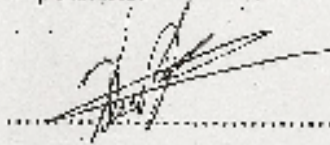
am Institut: für Thermodynamik und Energiewandlung
Betreuer: As. Univ. Prof. Dipl.-Ing. Dr. Reinhard Willinger
Studierende(r): Charalampos CHONDROKOSTAS
Kennzahl: E700 Matr.Nr.: 04 27 154
Thema der Diplomarbeit: Calibration of Pneumatic Five-Hole Probes in the
Free-Jet Wind Tunnel

KURZFASSUNG: Pneumatic pressure probes are a reliable and robust tool for flow field measurements in turbomachinery components. Prior to the measurement in the turbomachine, the probe has to be calibrated regarding the magnitude and the direction of the flow in a free jet wind tunnel. After the calibration task, nondimensional coefficients (calibration coefficients) are derived from the measured pressures at the probe sensing holes. Among the factors influencing the calibration of pneumatic pressure probes, the head geometry and the Reynolds number are the most important ones. Furthermore, the behaviour of the probe depends on the Mach number as well as on the turbulence intensity. Five-hole pressure probes can be used for three dimensional flow measurements. The scope of the present work is the investigation of the influence of various head geometries (cone probe, prismatic probe) and Reynolds numbers ($Re = 6.500$ and 13.000) on the calibration coefficients. Special attention is paid on the two different five-hole pressure probes. The experimental results from the free-jet wind tunnel are compared with the streamline projection method. The results of the present investigation supply the framework for the proper selection of a five-hole pressure probe geometry for the application in turbomachinery components.

5.12.2005

Willinger R.

Datum, Unterschrift des Betreuers



Unterschrift des(r) Studierenden

ΔΙΠΛΩΜΑΤΙΚΗ ΕΡΓΑΣΙΑ

ΘΕΜΑ: ΒΑΘΜΟΝΟΜΗΣΗ ΠΝΕΥΜΑΤΙΚΟΥ ΑΙΣΘΗΤΗΡΑ ΠΕΝΤΕ ΟΠΩΝ ΣΕ ΑΕΡΟΔΥΝΑΜΙΚΗ ΣΗΡΑΓΓΑ ΕΛΕΥΘΕΡΗΣ ΔΕΣΜΗΣ

ΠΕΡΙΛΗΨΗ ΘΕΜΑΤΟΣ

Οι πνευματικοί αισθητήρες αποτελούν ένα αξιόπιστο και ανθεκτικό εργαλείο για μετρήσεις του πεδίου ροής σε εξαρτήματα στροβιλομηχανών. Της διαδικασίας μετρήσεων στις στροβιλομηχανές, προηγείται η βαθμονόμηση του αισθητήρα σε σχέση με την ταχύτητα και την διεύθυνση της ροής, σε μια αεροδυναμική σήραγγα ελεύθερης δέσμης. Από τις μετρούμενες πιέσεις στις οπές του αισθητήρα προκύπτουν οι συντελεστές βαθμονόμησης (calibration coefficients). Οι σημαντικότεροι παράγοντες που επηρεάζουν τη βαθμονόμηση των αισθητήρων είναι η γεωμετρία της κεφαλής του αισθητήρα και ο αριθμός Reynolds. Επιπλέον, η συμπεριφορά του αισθητήρα εξαρτάται από τον αριθμό Mach καθώς επίσης και από την ένταση της τύρβης. Οι αισθητήρες πέντε οπών μπορούν να χρησιμοποιηθούν για τη μέτρηση της ροής σε τρεις διαστάσεις. Αντικείμενο της παρούσας έρευνας αποτελεί η μελέτη της επίδρασης της γεωμετρίας διαφόρων κεφαλών του αισθητήρα (κωνική, πρισματική) και του αριθμού Reynolds ($Re=6.500$ και $Re=13.000$) στους συντελεστές βαθμονόμησης. Ιδιαίτερη προσοχή δίνεται στη σύγκριση μεταξύ των δυο διαφορετικών αισθητήρων. Τα πειραματικά αποτελέσματα συγκρίνονται με τα θεωρητικά που προκύπτουν από τη μέθοδο απεικόνισης γραμμών ροής (streamline projection method). Το πόρισμα της εργασίας παρέχει το πλαίσιο επιλογής αισθητήρα με την κατάλληλη γεωμετρική κεφαλή για την πραγματοποίηση μετρήσεων σε εξαρτήματα στροβιλομηχανών.

ΠΕΡΙΛΗΨΗ ΔΙΠΛΩΜΑΤΙΚΗΣ ΕΡΓΑΣΙΑΣ

Οι πνευματικοί αισθητήρες αποτελούν ένα χρήσιμο εργαλείο κατά τη μελέτη του πεδίου ροής σε θερμικές στροβιλομηχανές και σε αεροδυναμικές εφαρμογές. Οι πνευματικοί αισθητήρες πέντε οπών χρησιμοποιούνται για μελέτη της ροής σε τρισδιάστατο επίπεδο. Η μετρούμενη πίεση στις οπές του αισθητήρα χρησιμοποιείται για τον υπολογισμό της ταχύτητας και της διεύθυνσης της ροής με έμμεσο τρόπο.

Της διαδικασίας μετρήσεων στις στροβιλομηχανές, προηγείται η βαθμονόμηση του αισθητήρα σύμφωνα με τις δεδομένες τιμές της ταχύτητας και της διεύθυνσης της ροής. Κατά τη διαδικασία της βαθμονόμησης χρησιμοποιείται μια αεροδυναμική σήραγγα ανοιχτού κυκλώματος. Ο αισθητήρας τοποθετείται σε προκαθορισμένες θέσεις συγκεκριμένης γωνίας μπροστά από την αεροδυναμική σήραγγα, με ροή σταθερής ταχύτητας και χαμηλή ένταση της τύρβης. Από τις μετρούμενες πιέσεις στις οπές του αισθητήρα προκύπτουν οι συντελεστές βαθμονόμησης.

Οι σημαντικότεροι παράγοντες που επηρεάζουν τη βαθμονόμηση των αισθητήρων είναι η γεωμετρία της κεφαλής του αισθητήρα και ο αριθμός Reynolds. Επιπλέον, η συμπεριφορά του αισθητήρα εξαρτάται από τον αριθμό Mach καθώς επίσης και από την ένταση της τύρβης

Αντικείμενο της παρούσας έρευνας αποτελεί η μελέτη της επίδρασης της γεωμετρίας διαφόρων κεφαλών του αισθητήρα πέντε οπών και του αριθμού Reynolds στους συντελεστές βαθμονόμησης. Ιδιαίτερη προσοχή έχει δοθεί στο σχεδιασμό, την εκτέλεση και την αξιολόγηση του πειράματος που διεξήχθη στην αεροδυναμική σήραγγα του εργαστηρίου του Τομέα Θερμοδυναμικής και Μετατροπής Ενέργειας (Institute of Thermodynamics and Energy Conversion) του Πολυτεχνείου της Βιέννης (T.U. Wien). Οι αισθητήρες πέντε οπών που διατίθενται καθώς και τα κύρια χαρακτηριστικά τους περιγράφονται αναλυτικά. Κάθε τύπος αισθητήρα παρουσιάζει συγκεκριμένα πλεονεκτήματα και μειονεκτήματα ανάλογα με τις εκάστοτε απαιτήσεις μετρήσεων στα εξαρτήματα των στροβιλομηχανών.

Επιπλέον της πειραματικής βαθμονόμησης, χρησιμοποιούνται απλές αναλυτικές εξισώσεις για τον υπολογισμό των συντελεστών βαθμονόμησης, από θεωρητικής άποψης (streamline projection method).

Το πόρισμα της εργασίας παρέχει το πλαίσιο επιλογής αισθητήρα με την κατάλληλη γεωμετρική κεφαλή για την πραγματοποίηση μετρήσεων σε εξαρτήματα στροβιλομηχανών.

ΔΙΑΡΘΡΩΣΗ ΔΙΠΛΩΜΑΤΙΚΗΣ ΕΡΓΑΣΙΑΣ

Στα πρώτα κεφάλαια της εργασίας γίνεται μια θεωρητική ανάλυση των εννοιών που θα χρησιμοποιηθούν παρακάτω. Πιο συγκεκριμένα, στα πρώτο κεφάλαιο, γίνεται εισαγωγή στην έννοια του πνευματικού αισθητήρα πέντε οπών καθώς και των μεθόδων θεωρητικής προσέγγισης και ανάλυσης των φαινομένων που προκύπτουν, ενώ στο δεύτερο κεφάλαιο, δίδονται οι μαθηματικοί τύποι που χρησιμοποιούνται για τον προσδιορισμό των πιέσεων και της θερμοκρασίας, καθώς και ο ορισμός των συντελεστών βαθμονόμησης όπως αυτοί χρησιμοποιήθηκαν παρακάτω.

Στο τρίτο κεφάλαιο ακολουθεί η αναλυτική παρουσίαση των τριών αισθητήρων που χρησιμοποιήθηκαν στο πείραμα. Από τους τρεις αισθητήρες που διαθέτει το Πολυτεχνείο της Βιέννης, οι δυο είναι κωνικής κεφαλής, πανομοιότυπης γεωμετρίας, με μοναδική διαφοροποίηση στο μήκος του στελέχους του αισθητήρα, ενώ ο τρίτος είναι πρισματικής κεφαλής με αρκετά ιδιόμορφη γεωμετρία. Αξίζει να σημειωθεί ότι οι δυο πρώτοι αισθητήρες, τσέχικης προέλευσης κατασκευάστηκαν κατά παραγγελιά, ενώ ο τρίτος είναι του εμπορίου με αμερικάνικη προέλευση. Για το λόγο αυτό, δεν γίνεται να αποκαλυφθούν οι κατασκευαστικές του λεπτομέρειες, παρόλο που οι περισσότερες μας έχουν γνωστοποιηθεί από την κατασκευάστρια εταιρία (UNITED SENSORS), για τους σκοπούς του πειράματος. Αντίθετα, στην περίπτωση των δυο άλλων αισθητήρων, όλα τα γεωμετρικά και κατασκευαστικά χαρακτηριστικά είναι γνωστά, αφού είναι ειδικής κατασκευής, και τα σχέδια για την κατασκευή τους δόθηκαν από τον καθηγητή R. Willinger.

Στο τέταρτο κεφάλαιο γίνεται θεωρητική προσέγγιση των μεγεθών που θα μετρηθούν πειραματικά, βάσει της μεθόδου απεικόνισης των γραμμών ροής (STREAMLINE PROJECTION METHOD). Η μέθοδος αυτή χρησιμοποιεί γνωστές μαθηματικές εξισώσεις, που σε συνδυασμό με την γεωμετρική ανάλυση στην κεφαλή του αισθητήρα, δίνει χρήσιμες μαθηματικές εκφράσεις για τους συντελεστές βαθμονόμησης όπως αυτοί ορίστηκαν καθώς και για τις πιέσεις που γίνονται αισθητές σε κάθε οπή του αισθητήρα. Κατόπιν, κάνοντας χρήση του προγράμματος Sigma Plot γίνεται γραφική απεικόνιση των θεωρητικών αποτελεσμάτων τα οποία εν συνεχεία θα συγκριθούν με τα πειραματικά για να εξαχθούν χρήσιμα συμπεράσματα για την αξιοπιστία και την κατάσταση στην οποία βρίσκονται οι αισθητήρες μας. Όπως γίνεται εύκολα αντιληπτό, η μέθοδος αυτή μπορεί να εφαρμοστεί μόνο στους αισθητήρες κωνικού τύπου, μιας και η ιδιόμορφη γεωμετρία κεφαλής του πρισματικού αισθητήρα, δεν επιτρέπει την θεωρητική προσέγγιση με ασφαλή και αξιόπιστα συμπεράσματα.

Η περιγραφή του πειράματος και ο εξοπλισμός που διαθέτει το εργαστήριο του Πολυτεχνείου της Βιέννης γίνεται στο πέμπτο κεφάλαιο. Τα τεχνικά χαρακτηριστικά της αεροδυναμικής σήραγγας αναφέρονται αναλυτικά. Μπροστά από το στόμιο της αεροδυναμικής σήραγγας τοποθετείται ο αισθητήρας πάνω σε μια κατασκευή η οποία επιτρέπει στην κεφαλή του να αλλάζει γωνίες χειροκίνητα στο οριζόντιο και στο κατακόρυφο επίπεδο. Το εύρος το οποίο θα εξετάσουμε είναι από -30° έως $+30^\circ$ σε κάθε επίπεδο, για πεδία ροής με αριθμό Reynolds $Re=6.500$ και $Re=13.000$. Μετά από αυτή την

κλίση παρατηρούνται φαινόμενα αποκόλλησης της ροής που ξεφεύγουν από το αντικείμενο μελέτης της εργασίας. Η πίεση που λαμβάνεται από κάθε οπή του αισθητήρα μετατρέπεται μέσω πιεζοηλεκτρικών κρυστάλλων σε ηλεκτρικό σήμα, το οποίο μέσω μονάδας ανάκτησης δεδομένων μεταφέρεται στον Η/Υ. Εν συνεχεία γίνεται η επεξεργασία των δεδομένων με το πρόγραμμα LabVIEW 5.0. Τέλος, με δεδομένα εισόδου αυτή τη φορά αυτά που προκύπτουν από το LabVIEW 5.0 γίνεται εκ νέου επεξεργασία με FORTRAN 77 ώστε να εξαχθούν για κάθε θέση οι συντελεστές κάθε οπής (κ_i , $i=1-5$), οι συντελεστές κατεύθυνσης (κ_β , κ_γ) καθώς και οι συντελεστές ολικής και στατικής πίεσης, κ_t και κ_s αντίστοιχα. Ο αριθμός Reynolds, ο αριθμός Mach και η ταχύτητα ροής V είναι δεδομένα. Ο σχεδιασμός των γραφημάτων γίνεται με το Sigma Plot

Στο έκτο και τελευταίο κεφάλαιο γίνεται η διεξοδική ανάλυση των αποτελεσμάτων και διάφορες συγκρίσεις μεταξύ i) πειραματικών και θεωρητικών μεθόδων, ii) διαφορετικών αριθμών Reynolds, και iii) των τριών αισθητήρων. Ακολουθεί εξήγηση για τις ασυμφωνίες και τις διαφοροποιήσεις των διαγραμμάτων, καθώς και εκτενής αναφορά στους παράγοντες που επηρεάζουν τη βαθμονόμηση αισθητήρων. Από την πειραματική διαδικασία, προκύπτουν χρήσιμα συμπεράσματα για την καταλληλότητα κάθε αισθητήρα (κάποιοι από αυτούς δεν έχουν χρησιμοποιηθεί για περισσότερα από δέκα έτη) καθώς και για τα πλεονεκτήματα ή μειονεκτήματα που παρουσιάζει κάθε τύπος ανάλογα με τη χρήση που προορίζεται.

Η διπλωματική εργασία εκπονήθηκε στο Πολυτεχνείο της Βιέννης το χρονικό διάστημα Μάρτιος- Δεκέμβριος 2005, και βρίσκεται στο site του Τομέα Θερμοδυναμικής και Μετατροπής ενέργειας (Intitute für Thermodynamik and Energiewandlung, ITE)στην ακόλουθη διεύθυνση:

http://www.ite.tuwien.ac.at/teaching/bachelor_diploma_theses/finished_bt_mt/EN/# στο Year 2005

ή αλλιώς στη σελίδα

http://www.ite.tuwien.ac.at/typo3conf/ext/user_tuwien_links/download.php?cuid=8157&file=fileadmin%2Ft%2Fite%2FLehre%2FDiplomarbeiten%2F2005%2FChondrokostas.pdf

Επισυνάπτεται η διπλωματική εργασία στα Αγγλικά.....



TECHNISCHE
UNIVERSITÄT
WIEN

VIENNA
UNIVERSITY OF
TECHNOLOGY



DIPLOMA THESIS

Calibration of Pneumatic Five-Hole Pressure Probes In the Free-Jet Wind Tunnel

conducted at
Institute of Thermodynamics and Energy Conversion
Vienna University of Technology

under the direction of
Ao. Univ. Prof. Dipl.-Ing. Dr. techn. R. WILLINGER

under the responsibility of
Professor S.TSANGARIS
on behalf of N.T.U.A.

by
Charalampos CHONDROKOSTAS

Vienna, December 2005

Acknowledgements

First of all, I would like to take this opportunity to thank Professors S.TSANGARIS and R.WILLINGER for awarding me the opportunity to conduct my research and write this paper at the Institute of Thermodynamics and Energy Conversion of the Vienna University of Technology.

Furthermore I would especially like to thank Prof. Reinhard WILLINGER for his guidance, empathy, the ideal working conditions with which he provided me and moreover for his precious time.

Additionally, I would like to offer my thanks to Cornelius and Natalie for their precious support in order to revise and finalize this work.

I am extremely glad that I have been granted such a rewarding and fulfilling experience this year in Vienna.

Η παρούσα εργασία, αποτελεί προσπάθεια ανταπόδοσης και ευχαριστίας, σε όλους εκείνους που στάθηκαν στο πλάι μου καθ' όλη την πορεία μου μέχρι τώρα, και στήριξαν με τον καλύτερο δυνατό τρόπο τις αποφάσεις μου.

Abstract

Pneumatic probes are still a useful tool when investigating flow fields within thermal turbomachines, cascades or any other aerodynamic facility. Five-hole pressure probes can be used for three-dimensional flow studies. The pressures sensed at the probe holes are used for the estimation of the velocity and direction of the flow in an indirect manner.

Prior to the measurement in the turbomachine, the probe has to be calibrated according to the expected values of the velocity and direction. An open jet wind tunnel is used for this calibration task. The pressure probe is positioned at a number of predefined angular settings in a free jet with constant velocity and low turbulence intensity. After the calibration task, some calibration coefficients are obtained from the measured pressures at the probe sensing holes.

Among the factors influencing the calibration of pressure probes, the head geometry and the Reynolds number are the most important ones. Furthermore, the behaviour of the probe depends on the Mach number as well as the turbulence intensity.

The scope of the present diploma thesis is the investigation of the influence of various head geometries and Reynolds numbers on the calibration coefficients of five-hole pressure probes. Special attention has been paid in the planning, execution and evaluation of experiments in the free jet wind tunnel of the Institute of Thermodynamics and Energy Conversion of the Vienna University of Technology (T.U. Wien). The five-hole probe head geometries available in the institute and their main characteristics are described in this work. Each probe has its specific advantages and disadvantages concerning the application in components of turbomachines.

In addition to the experimental calibration, simple analytical expressions have been deduced for the estimation of the calibration coefficients, at least qualitatively.

The results of the present investigation should supply the framework for the proper selection of five-hole pressure probe geometry for the application in turbomachinery components.

Table of Contents

| | |
|--|-----------|
| 1. Introduction | 1 |
| 1.1. Five-hole pressure probes | 2 |
| 1.2. Theoretical analysis methods..... | 3 |
| 2. Calibration | 4 |
| 2.1. Experimental calibration for five-hole probe | 4 |
| 2.2. Energy Bernoulli equation | 5 |
| 2.3. Definition of hole and calibration coefficients | 7 |
| 2.4. Temperature measurement..... | 9 |
| 3. Five-Hole Probes Geometry | 11 |
| 3.1. SVUSS/5 conical probe..... | 13 |
| 3.2. DA-125-18-F-16-C (prismatic probe)..... | 17 |
| 3.3. DA-125-24-F-22-C (prismatic probe)..... | 19 |
| 4. Streamline Projection Method | 20 |
| 4.1. Conical probe head geometry | 21 |
| 4.2. Prismatic shaped probes..... | 25 |
| 5. Test Facility | 26 |
| 5.1. Description of the wind tunnel | 26 |
| 5.2. Experimental calibration..... | 28 |
| 5.3. Flow velocity field | 31 |
| 6. Results and Discussion | 34 |
| 6.1. Comparison of theoretical and experimental results -Reynolds number and Mach number effects..... | 35 |
| 6.1.1. SVUSS/5 conical probe | 35 |
| 6.1.2 Prismatic five-hole probe (<i>United Sensor</i>) | 42 |
| 6.2. Comparison between probes | 48 |
| 6.3. Other factors influencing the calibration of five hole probe..... | 53 |
| 6.3.1. Hole geometry for static pressure taps | 53 |
| 6.3.2. Turbulence intensity | 53 |
| 6.3.3. Velocity gradient effects | 54 |
| 6.3.4. Wall proximity effects | 54 |
| 6.3.5. Influence of probe supports | 55 |

Endnote I

| | |
|---------------------------|----|
| FORTTRAN 77 program | 56 |
|---------------------------|----|

Endnote II

| | |
|----------------------------|----|
| Hole numbering order | 59 |
|----------------------------|----|

| | |
|---------------------|----|
| Bibliography | 61 |
|---------------------|----|

| | |
|---------------------|----|
| Picture list | 62 |
|---------------------|----|

| | |
|-------------------|----|
| Table list | 63 |
|-------------------|----|

Nomenclature

| | | |
|-----------|-----------|--|
| a | [m] | side hole spacing |
| A | [m^2] | cross-sectional area |
| A_p | [m^2] | nozzle exit area |
| A_n | [m^2] | probe head blockage area |
| B | [-] | total blockage |
| D | [m] | probe width |
| d_n | [m] | nozzle diameter |
| k_i | [-] | hole coefficient |
| \bar{k} | [-] | mean hole coefficient |
| k_β | [-] | direction coefficient |
| k_t | [-] | total pressure coefficient |
| k | [-] | static pressure coefficient |
| Ma | [-] | Mach number |
| N | [1/min] | rotational speed |
| p | [Pa] | static pressure |
| \bar{p} | [Pa] | mean pressure |
| p_i | [Pa] | pressure sensed by the hole i |
| p_{ref} | [Pa] | reference pressure |
| p | [Pa] | total pressure |
| Pr | [-] | Prandtl number |
| r | [-] | recovery factor |
| Re | [-] | Reynolds number |
| S | [m] | distance along streamline |
| t | [s] | time |
| T | [K] | flow temperature |
| T_0 | [K] | thermodynamically ideal stagnation temperature |
| T_{pi} | [K] | ideal probe temperature |
| T_{ref} | [K] | environmental temperature |

| | | |
|---------------------|-----------------------------------|--|
| T_s | [K] | fluid static temperature |
| T_w | [K] | ideal dynamic temperature |
| V | [m/s] | velocity |
| V_0 | [m/s] | speed of sound in undisturbed medium |
| \bar{V}_n^2 | [m ² /s ²] | resultant turbulence intensity |
| x | [m] | distance downstream of the nozzle exit plane |
| $\Delta\beta$ | [°] | yaw angle |
| $\Delta\gamma$ | [°] | pitch angle |
| $\Delta\varepsilon$ | [°] | flow angle error |
| Δp | [Pa] | pressure difference |
| δ | [°] | wedge angle, characteristic angle |
| φ | [°] | angular coordinate |
| λ | [W/(m · K)] | thermal conductivity |
| μ | [kg/(m · s)] | dynamic viscosity |
| ν | [m ² /s] | kinematic viscosity |
| ρ | [kg/m ³] | density |

Subscripts

| | |
|---------|-------------------------------------|
| d | related to probe diameter |
| $i=1-5$ | related to hole number |
| x,y | related to the X-axis or the Y-axis |

Abbreviations

| | |
|-------|------------------------------|
| $3D$ | three-dimensional |
| CFD | computational fluid dynamics |
| spm | streamline projection method |

1. Introduction

It is not difficult to think about several general needs for flow measurements. In some cases, the data are useful themselves. In these cases, the flow quantity desired should be measured either directly or indirectly and this would be the final result. In other cases, flow measurements are necessary for correlation of dependent variables.

The many applications of fluid flow measurements cover a broad spectrum of activities. For example, it is possible to consider various wind-tunnel studies related to lift and drag, vibration, and noise radiation. In engine and compressor research involving both reciprocating and rotating machinery and in the broad area of hydraulic engineering research, many different types of flow measurements are necessary.

In addition, many basic types of testing require fluid mechanics measurements, including cooling studies, the design of hydraulic systems, engine tests, flow calibration facilities, and of course, matters related to turbomachinery.

Physical modelling is still very useful in many branches of engineering, ranging from wind-tunnel tests of airplanes and other aerospace vehicles, buildings, diffusion of pollutants, windmills, and even snow fences to hydraulic models of entire dams, reaches of rivers and cooling-water intakes and outlets. Many of these applications require specialized instrumentation.

It is essential to understand fluid mechanics for the design of experiments, for the interpretation of results, and for estimating deterministic errors due to the flow modification by instrumentation placed in the flow.

First, it is required to know the purpose of the measurements. Secondly, the fluid mechanics of the problem should be understood. Almost all types of measurement techniques depend on the nature of the flow, and this in turn governs instrument selection. The physical principles involved in flow measurements should also be understood. Almost all fluid flow measurements are indirect. In that, the techniques rely on the physical interpretation of the quantity measured.

It is easy to see the interrelated roles of flow instrumentation, the theory of fluid mechanics, and of research and development. The need for a clear understanding of the problem, the principles of fluid mechanics, the principles of operation of the flow instrumentation, and the elements of statistical analysis is evident.

1.1. Five-hole pressure probes

In many complex flow fields such as those encountered in turbomachines, the experimental determination of the steady state three-dimensional characteristics of the flow is frequently required. But in contrast to the free jet, the flow field in a turbomachinery component exhibits strong velocity gradients, induced by the blade wakes as well as by the hub and casing boundary layers.

Continued development of turbomachine technology is dependent on the experimental determination of the performance of advanced components. The primary measurements in turbines and compressors consist of flow direction and total and static pressures as well as total and static temperatures.

Flow velocity field and pressure distribution are two valuable variables alone. They can be used for verification of theory. A great deal of experimental data is necessary for calibrating mathematical models of various types. But the measurement of velocity and pressure in a flowing system can also be useful as a diagnostic for determining various quantities. For example, velocity measurements are often used in problems related to noise and vibration and as a diagnostic in heat and mass transfer research.

The harsh turbomachine environment makes five-hole pressure probes particularly attractive for the measurement of flow pressure, velocity and direction. On the other hand, these types of probes are becoming more useful with the development of small inexpensive fast response pressure transducers, computer controlled traversing systems, and computer based data acquisition and analysis.

The five-hole pressure probes available in the Institute of Thermodynamics and Energy Conversion of the Vienna University of Technology (T.U. Wien) have two different head geometries. Each type of probe has its specific advantages and disadvantages concerning the application in components of turbomachines.

Differential pressure measurements provide a useful alternative to hot-wire and hot-film anemometry for determining complex flow directions and even turbulence intensity. Separate measurements of the total and static pressures can yield both the mean and fluctuating components of velocity and pressure.

1.2. Theoretical analysis methods

It would be advantageous if the calibration characteristics and response of a five-hole probe could be determined by analytical procedures. In fact, there are methods that can help to face up the analysis of pressure probes from a theoretical viewpoint. One of these methods is *the streamline projection method*.

For probes with complex head geometries such as prism probes, analytical procedures of any type are difficult. These complex geometries, characterized by abrupt changes in contour, are subject to flow separation and viscous effects that are not modelled by current computational techniques. Nevertheless, the streamline projection method is used in addition to the experimental research as well as the computational investigations. It will be shown that this simple method can easily predict the five-hole probe calibration coefficients, at least qualitatively.

For probes of simple contour geometry, (e.g., conical probe head), the streamline projection method is valid. Although the analytic relationship is valuable for characterisation of probe behaviour and as a guide to the functional form of calibration equations, it is unlikely that they are capable of replacing individual probe calibrations. This is due to both the limitations of the derivation as well as the manufacturing irregularities of the probes. Regardless of the accuracy of the theoretical derivations, the latter effects may always necessitate individual probe calibrations, particularly for small sized probes.

Measurement of data and development of an interpolation procedure for the data analysis become the responsibility of the probe user.

2. Calibration

The objective of an aerodynamic probe - in the present context - is to determine the scalar and vector properties of complicated flow fields such as those encountered around complex bodies or in turbomachines, in terms of static and total pressure and three-dimensional (3D) velocity components respectively. This translates into a measurement of pressures, which by means of calibration functions and gas dynamic relationships, are subsequently converted into flow angles and Mach numbers.

Five-hole pressure probes, of many different configurations, are frequently used for three-dimensional flow measurements in turbomachinery components. They yield the total as well as the static pressure and the direction of the flow field. But as it was said before, due to manufacturing inaccuracies a calibration procedure prior to the measurements is necessary.

Pressure differentials are then measured for selected angles of yaw and pitch placed on the probe relative to the flow direction. When compressibility is not a consideration, the theory yields a format for interpreting the differential pressures between pairs of holes as functions of angles of pitch and yaw. Once the flow direction has been established, the remaining pressure and hence velocity data may be determined from further coefficients.

2.1. Experimental calibration for five-hole probe

The five hole probes employed in this study were used in a fixed position or non-nulling mode. This method is not that accurate but offers simplicity in installation. The latter characteristic is the most important in turbomachine applications.

It is performed by setting the probe at constant pitch and yaw values with respect to the test section. The five pressures are measured at each measurement location by traversing the probe over the flow field. From these five measured pressures,

the direction and magnitude of the flow with respect to the X-axis of the pressure probe are determined.

Although elegant in its simplicity, this technique encounters singularity when calibration for large angle of pitch or yaw is sought [6]. So it is restricted to lower flow angle ranges, preventing its use in highly 3D flows.

2.2. Energy Bernoulli equation

The flow motion is known to be a function of several non-dimensional parameters. The most important ones in aerodynamics are:

Reynolds number:

$$Re = \frac{\text{Inertial force}}{\text{Viscous force}} = \frac{V \cdot d}{\nu} \quad (1)$$

Mach number:

$$Ma = \frac{\text{Inertial force}}{\text{Elastic force}} = \frac{V}{V_0} \quad (2)$$

Gases at low Mach number - the calibration experiments are conducted at $Ma < 0.2$ - can be considered as essentially incompressible (constant-density) fluids. The analysis of the steady flow for this sort of fluid [3] starts with the conservation of mass, momentum and energy.

For one-dimensional flow along a stream tube (Fig. 1), the mass conservation equation for steady flow has the form:

$$V \cdot A = \text{const} \quad (3)$$

If it is further assumed that the flow is inviscid, the momentum equation is:

$$\frac{\partial p}{\partial s} + \rho \cdot V \cdot \frac{\partial V}{\partial s} + \rho \cdot \frac{\partial V}{\partial t} = 0 \quad (4)$$

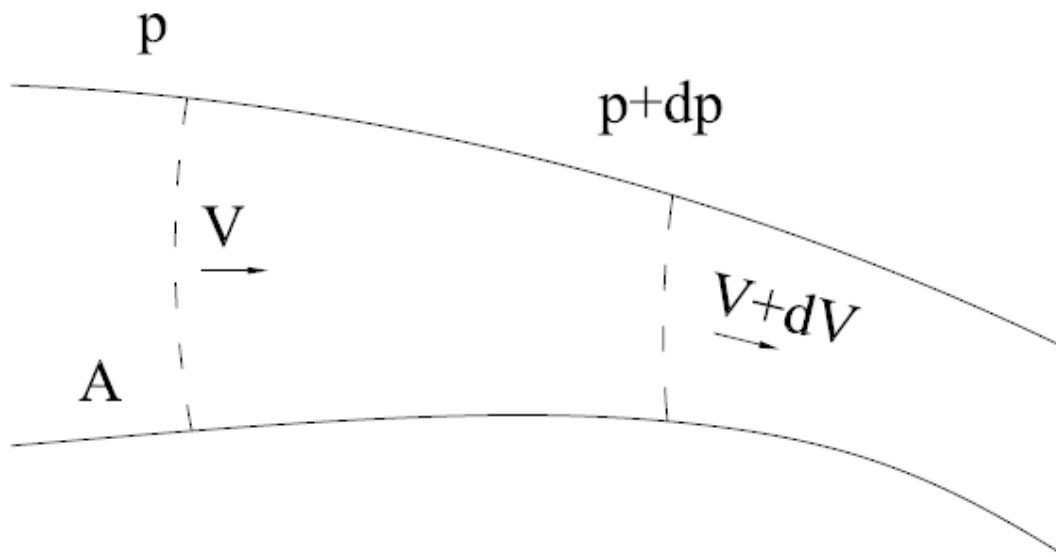


Fig 1: Inviscid flow along a stream tube

The cross section of the stream tube must be small in order to consider the local values of the pressure and velocity.

For the steady state, the last term in Eq. (4) drops out, and the equation can be integrated along the direction s of the stream tube, to result in the Bernoulli conservation equation for energy:

$$p + \rho \cdot \frac{V^2}{2} = \text{const} \quad (5)$$

The pressure p in Eq (5) is the static pressure. It is the component of the pressure that represents fluid hydrostatic effects. In principle, it is measured by an instrument that moves along with the fluid. This is, however, inconvenient, and the pressure is usually measured via a small hole in a wall arranged so that it does not disturb the flow. The quantity $\rho \cdot \frac{V^2}{2}$ is usually called dynamic pressure. It is the component of the fluid that represents fluid kinetic energy.

Total pressure p_t , sometimes also called “stagnation pressure”, is defined as the pressure that would be reached if the local flow is *imagined* to slow down to zero velocity, frictionless. Total pressure is the sum of static and dynamic pressure:

$$p_t = p + \rho \cdot \frac{V^2}{2} \quad (6)$$

From measurements of the total and static pressures, the velocity can be obtained as,

$$V = \sqrt{\frac{2}{\rho} \cdot (p_t - p)} \quad (7)$$

which follows readily from Eq. (6).

For Eqs. (6) and (7) to apply, the probe must not disturb the flow, and it must be carefully aligned parallel to the stream.

2.3. Definition of hole and calibration coefficients

The pressure sensed by the hole i differs from the free stream static pressure p , and it can be presented as a nondimensional pressure coefficient. The **hole coefficient** k_i is usually used in the following form:

$$k_i = \frac{p_i - p}{\frac{\rho}{2} \cdot V^2} \quad (8)$$

where i represents the identifier of a specific hole between 1 and 5.

For operation in the non-nulling mode with a five-hole probe, it is apparent that the calibration characteristics must include data that represent pressure differences in the yaw plane as well as differences between the measured and the true, local total and static pressures. When the probe is used to measure these quantities, the relationship between them and the yaw angle $\Delta\beta$ or the pitch angle $\Delta\gamma$, is described by the calibration coefficients. These pressure coefficients must be defined so that they are independent of velocity and are a function only of the flow angularity.

Various definitions for the calibration coefficients can be found in the literature [6]. The use of these individual hole-based coefficients allows the flow phenomena to be investigated irrespective of the chosen calibration coefficient definitions.

The present work uses the standard accepted non-dimensional grouping for reducing the data. This is the definition by Treaster and Yocum [8]:

- **Direction coefficient k_β :**

$$k_\beta = \frac{p_2 - p_3}{p_1 - \bar{p}} = \frac{k_2 - k_3}{k_1 - \bar{k}} \quad (9)$$

- **Direction coefficient k_γ :**

$$k_\gamma = \frac{p_4 - p_5}{p_1 - \bar{p}} = \frac{k_4 - k_5}{k_1 - \bar{k}} \quad (10)$$

- **Total pressure coefficient k_t :**

$$k_t = \frac{p_1 - p_t}{p_1 - \bar{p}} = \frac{k_1 - 1}{k_1 - \bar{k}} \quad (11)$$

- **Static pressure coefficient k_s :**

$$k_s = \frac{\bar{p} - p}{p_1 - \bar{p}} = \frac{\bar{k}}{k_1 - \bar{k}} \quad (12)$$

Where the quantities:

$$\bar{p} = \frac{p_2 + p_3 + p_4 + p_5}{4} \quad (13)$$

and

$$\bar{k} = \frac{k_2 + k_3 + k_4 + k_5}{4} \quad (14)$$

represent the mean pressure and the mean hole coefficient, respectively.

As can be seen from Eqs. (9) to (12), the calibration coefficients are related directly to the five hole coefficients.

Treaster and Yocum found that an indicated dynamic pressure formed by the difference between the indicated total pressure p_1 , and the averaged value of the four indicated static pressures p_2 , p_3 , p_4 and p_5 , was a satisfactory normalizing parameter. It reduced the scatter in the calibration data as compared to using the true dynamic pressure. The difference of the two pressures $p_1 - \bar{p}$ is consequently taken to represent the dynamic pressure, which is used to make the calibration

pressure coefficients non-dimensional. This is convenient, since using the true dynamic pressure would have introduced an unknown quantity.

The problem with the Treaster and Yocum definition arises when there is a change in sign in the denominator, or more precisely when the denominator goes to zero producing a singularity that in turn makes the coefficients of yaw, pitch, total, and static pressure become infinite. That happens when in the non-nulling mode, for large angles of both yaw and pitch, p_1 and \bar{p} deviate significantly from the actual total and static pressure, and therefore, their difference no longer represents the dynamic pressure. It thus appears that the problem lies in the definition of the denominator of calibration coefficients.

In the last years, attempts to extend the calibration range for five-hole probes in the stationary method have been undertaken. Some works [6] have developed a modification to the denominator of the Treaster and Yocum calibration coefficients, which successfully allows calibration to much higher angles of yaw, while maintaining the simplicity of the original procedure.

2.4. Temperature measurement

The measurement of the temperature of a real fluid [3] generally consists of reading the output signal of a thermometer as the fluid stagnates against the sensor surface and equilibrates thermally with this sensor surface. Because of the viscous and thermal diffusion properties of real fluids, the thermometer generally does not indicate the thermodynamically ideal stagnation temperature

$$T_0 = T_s + T_w \quad (15)$$

where:

T_0 = thermodynamically ideal stagnation temperature

T_s = fluid static temperature

T_w = ideal dynamic temperature

The Prandtl number Pr expresses the ratio of fluid viscous to thermal diffusion effects. That is:

$$Pr = \frac{\text{Viscous effects}}{\text{Thermal diffusion}} = \frac{\mu \cdot c_p}{\lambda} \quad (16)$$

where:

μ = dynamic viscosity of fluid

λ = thermal conductivity

Thus when, as in air, with $0,65 < Pr < 0,7$ thermal diffusion effects are greater than the viscous effects, the real dynamic temperature is less than the ideal.

Of course, for $Pr=1$ the viscous heating effects generated by the stagnating real fluid are exactly diffused thermally so that the real dynamic temperature is the ideal.

Thus,

$$T_{pi} = T_s + r \cdot T_w \quad (17)$$

where:

$$\begin{aligned} T_{pi} &= \text{ideal probe temperature} \\ r &= \text{recovery factor} \end{aligned}$$

The recovery factor can then be written:

$$r = \frac{T_{pi} - T_s}{T_0 - T_s} \quad (18)$$

Therefore the temperature sensed by a sensor in a fluid stream depends upon:

1. The viscous and thermal diffusion properties.
2. The characteristics of the sensor, i.e., shape and orientation to the flow.
3. The nature of the fluid stagnation process, including any pertinent fluid motions effects, such as turbulence, that might alter the molecular viscous and thermal diffusion phenomena described above.
4. Any other kind of thermal losses from the temperature sensor.

3. Five-Hole Probes Geometry

Although a variety of pressure probes have been devised for decomposing the flow velocity vector, the most well known and widely used is the five-hole pressure probe. A flow direction probe is made up of a streamlined axisymmetric body that points into the flow. As the name implies, it is characterized by five pressure sensing holes.

The frequently adopted nomenclature and the convention used to number the five-hole pressure sensing holes are shown in Fig.2:

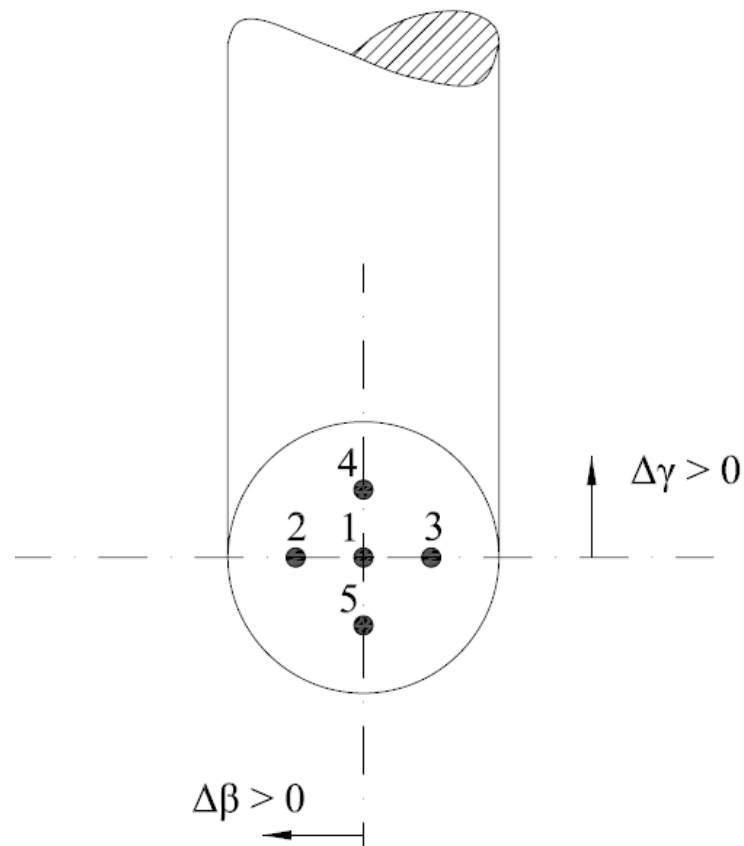


Figure 2: Adopted geometry nomenclature

The pitch and yaw planes orientation relative to the probe is independent of the device used to position the probes during calibration.

The angle defined between the velocity vector V and the velocity projection, over the yaw plane, is the yaw angle $\Delta\beta$, whilst the angle between the velocity projection over the yaw plane and the probe axis is the pitch angle $\Delta\gamma$.

The pressure distribution on the surface of the probe depends on the angle of incidence of the mean flow vector relative to the axis of the probe. To determine the three-dimensional orientation and magnitude of the flow vector, the surface pressure is sampled at five locations: on the axis of the probe and at two equispaced points on each plane of the probe.

The central pressure tap gives the conventional stagnation pressure when the flow vector is perpendicular to that point on the surface. The pressure difference between the pressure side sensing-holes per plane may be related to the inflow velocity vector by using an appropriate calibration to deduce the yaw and the pitch direction respectively.

The flow field parameters should be accurately measured with the probe, creating a minimal flow disturbance. Thus, the probe must consist of a slender body, i.e., the body radius must be much less than the body length. As long as the simple shape is small enough so that it does not disturb the flow, and the velocity over it is uniform yet large enough so that laminar separation does not generate any self-turbulence, the flow over it will be streamlined. On the other hand, in order to maximize their spatial resolution, such probes are generally miniaturized.

Since the probes are to be used without rotation, the sensitivity to flow direction (angularity) is extremely important. In addition to the probe sensitivity, alignment and manufacturing defects also influence the accuracy with which flow angles, static and total pressures can be determined.

Several different five-hole probe head geometries have been investigated. They are available in several configurations, such as prismatic, conical, pyramidal, cylindrical, spherical etc...

Three different types of five-hole probes are available in the Thermodynamics and Energy Conversion Institute of the Technical University of Vienna. Two of them are commercially available whilst one of them is a special order. These probes are listed below.

- **SVUSS/5** (conical probe)
- **DA-125-18-F-16-C** (prismatic probe)
- **DA-125-24-F-22-C** (prismatic probe)

Detailed information about these pneumatic five-hole probes is available on the following pages.

3.1. SVUSS/5 (conical probe)

The SVUSS/5 conical probe is shown in Fig. 3. It is manufactured by the company SVUSS (Prague - Czech Republic). The year of manufacture is 1994.

Its total length is 650 mm and it basically consists of five hypodermic tubes, which are bundled together. The tubes have an assembled diameter of 6 mm and they are ground to form the “goose neck” shaped head, with forward facing pressure tapings. The term *forward facing* refers to the axes of the holes. They are parallel to the axis of the probe, thus facing forward into the flow.



Figure 3: Five-hole SVUSS/5 conical probe

Fig. 4 shows the conical probe head geometry sketch, the numbering of the holes as well as the definition of the characteristic angle δ . The characteristic dimension of the probe head is d and the side holes are separated by the dimension α .

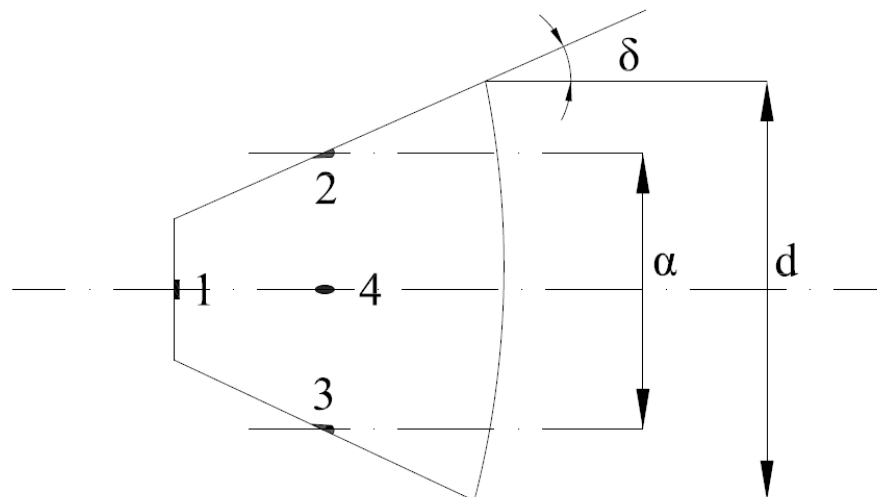


Figure 4: Conical five-hole probe head geometry

The characteristic diameter of the probe head (see Fig. 5 and Fig. 6) is $d=3\text{mm}$, and the wedge angle, between the probe axis and the direction parallel to the probe head sides, is $\delta=30^\circ$



Figure 5: SVUSS/5 conical probe head side view

The distance between the centres of the side holes on each axis is $1,85\text{ mm}$ and the diameter of the holes is $0,5\text{ mm}$

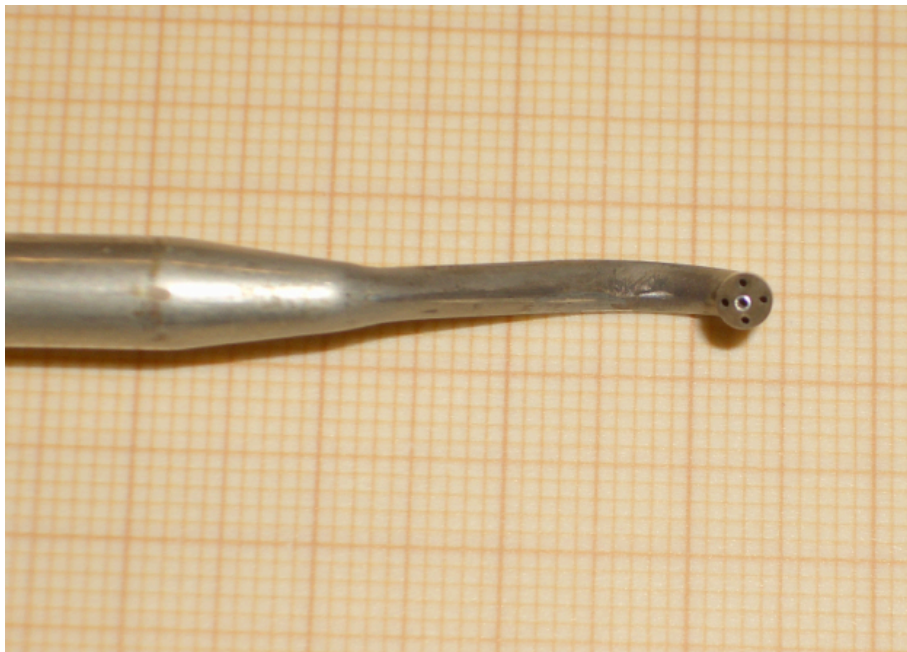


Figure 6: SVUSS/5 conical probe head front view

This model of probe includes no thermocouple to measure the flow temperature.

The current probe was a special order to the SVUSS Company which no longer exists. A detailed sketch of the probe with all manufacturing dimensions can be found on the following page.

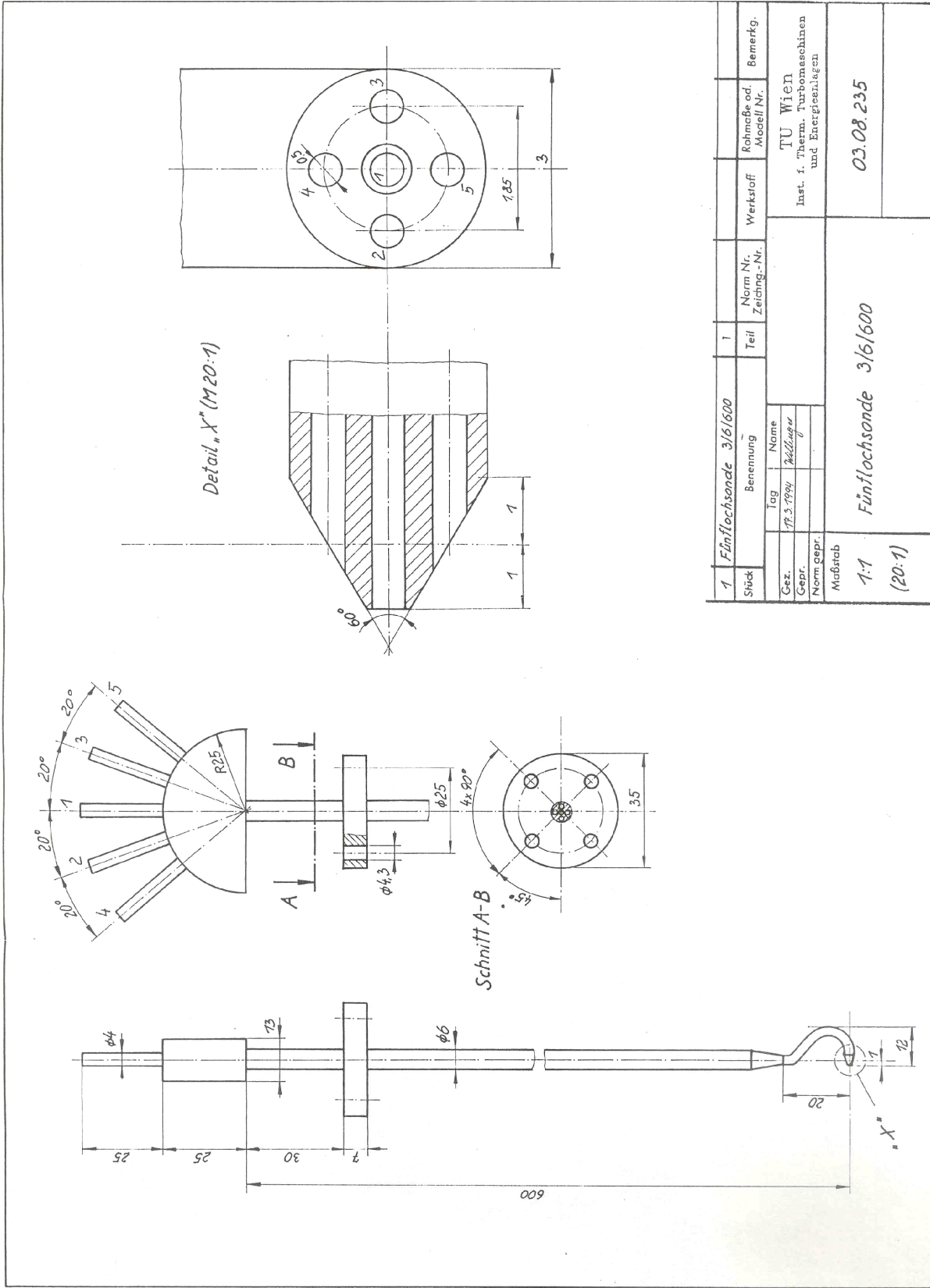
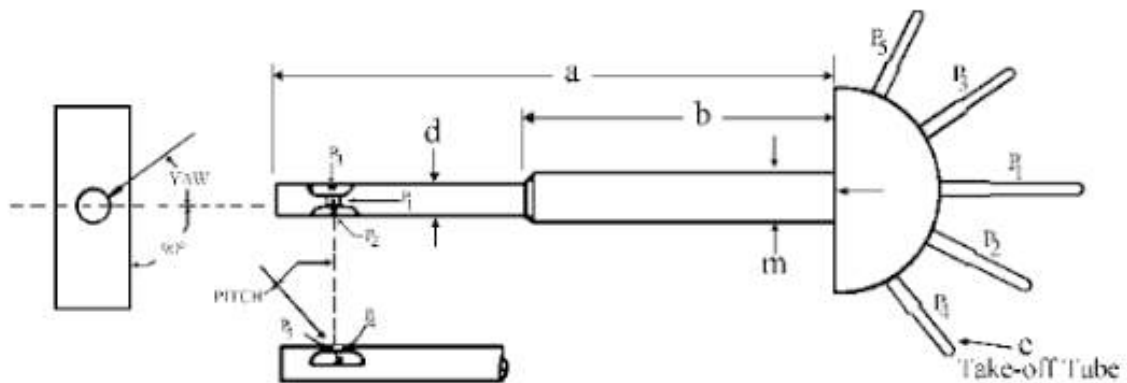


Figure 7: Sketch for the SVUSS/5 conical probe

3.2. DA-125-18-F-16-C (prismatic probe)

This commercial probe is designed and manufactured by *UNITED SENSOR*. Therefore the manufacturing characteristics as well as some of the geometrical characteristics are classified. In figure 8 the order form and the known dimensions of this probe are shown.

Ordering Information:



Typical Example: DAT-187-24-F-22-CD-K-Plug

| | | | | | | |
|------|--|-------|-------|-------|------|------|
| DAT: | Sensing Head Type * | | | | | |
| 187: | d = .187" - Sensing Head Diameter (inches) ** | | | | | |
| 24: | a = 24" - Overall Length (inches) | | | | | |
| F: | m = 1/4" Reinforcement Tubing Diameter *** | | | | | |
| | D | E | F | H | J | L |
| | 1/16" | 3/16" | 1/4" | 5/16" | 3/8" | 1/2" |
| 22: | b = 22" - Reinforcement tubing length (inches) *** | | | | | |
| CD: | e = 5/32" Swaged down to 1/8" - Take-off Tube Diameter | | | | | |
| | A | C | D | E | F | |
| | 1/16" | 1/8" | 5/32" | 3/16" | 1/4" | |

Thermocouple Type (DAT probe only)

| | |
|-------|--|
| K: | Chromel - Alumel Thermocouple |
| J: | Iron - Constantan |
| T: | Copper - Constantan |
| E: | Chromel - Constantan |
| Plug: | Plug termination is standard. Jacks or leadwire are available. - DAT probes only |

Figure 8: United Sensor ordering form

The overall length of the probe, as the form implies is 18" and the reinforcement tubing length is 16". The sensing head diameter is 0,125". An actual picture of the probe can be found in figure 9.



Figure 9: DA-125-18-F-16-C prismatic probe

Further information about the hole diameters, the characteristic angle and the hole spacing are not given but figures 10 and 11 are helpful in order to obtain a detailed view of the probe.



Figure 10: DA-125-18-F-16-C head front view



Figure 11: DA-125-18-F-16-C head side view

3.3. DA-125-24-F-22-C (prismatic probe)

This probe is similar to the DA-125-18-F-16-C probe. The only difference is on the reinforcement tube length which is 22" (6" longer) and as a consequence the overall length which is 24" (6" longer as well).

4. Streamline Projection Method

The streamline is defined as a curve everywhere tangent to the instantaneous velocity vectors (everywhere parallel to the instantaneous direction) of the flow. Thus, these curves provide a clear picture of the flow, because the velocity vector has at each point the direction of the streamline. For steady flow, the streamlines also describe the path that the fluid particles follow.

The streamline projection method is based on the assumption that the free stream velocity (which magnitude V is supposed to be constant) is projected on each one of the five sensing holes. Therefore, the velocity component normal to the probe surface results in a dynamic pressure, which is added to the free stream static pressure. Consequently, the holes of the probe measure a total pressure equal to the static pressure plus the corresponding fraction of the dynamic pressure. This is:

$$p_i = p + \frac{1}{2} \rho \cdot V_i^2 \quad i=1-5 \quad (19)$$

where V is the velocity projection normal to the hole i surface.

From the hole coefficient definition (Eq. (8)) can be obtained that:

$$p_i = p + \frac{k_i}{2} \cdot \rho \cdot V^2 \quad (20)$$

Comparison between Eqs. (19) and (20) makes it possible to rewrite the hole coefficient formula when the streamline projection method is being used.

$$k_i = \left(\frac{V_i}{V} \right)^2 \quad (21)$$

The velocity projection exclusively depends on the probe head geometry but can only be applied on simple and symmetrical ones. As a result of this, in this diploma thesis the streamline projection method can only be applied on the five hole conical

probe in order to obtain the five-hole probe's calibration coefficients, from a strict theoretical viewpoint. It should also be mentioned that even if the head geometry of the United Sensor probes was more simple and symmetrical, there would be difficulties in applying the method due to the fact that the geometrical-manufacturing characteristics are classified.

Moreover than just giving a first estimation of calibration coefficients for five-hole probes, the streamline projection method can also be used to estimate the influence of a velocity gradient on the flow angle measurement [10] with the same type of probes. However, that field of work is out of the scope of this diploma thesis.

4.1. Conical probe head geometry

The following random flow field is assumed (Fig 12). The yaw angle is $\Delta\beta$, the pitch angle is $\Delta\gamma$ and the characteristic angle is δ ($\delta=30^\circ$)

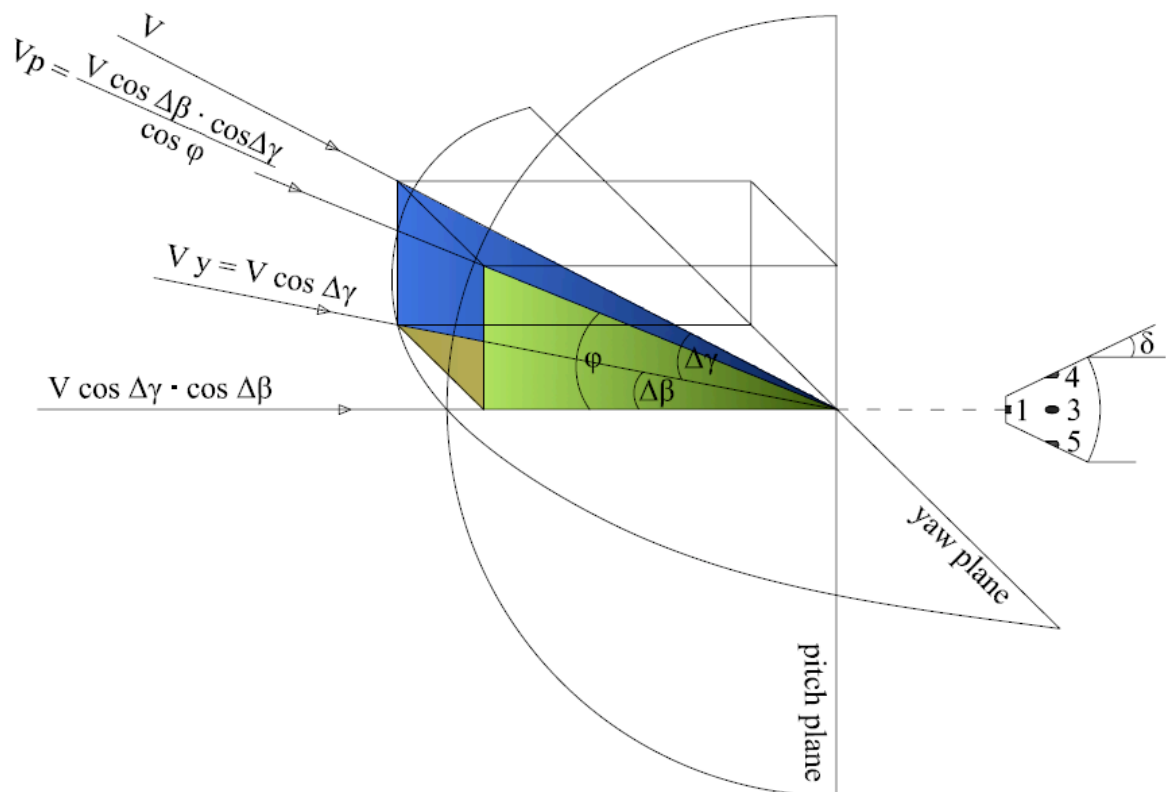


Figure 12: Flow velocity analysis

From the analysis of the velocity on the yaw and pitch plane, the following velocity expressions are obtained for each plane respectively:

$$V_y = V \cdot \cos \Delta\gamma \quad (22)$$

$$V_p = V \cdot \frac{\cos \Delta\beta \cdot \cos \Delta\gamma}{\cos \varphi} \quad (23)$$

where φ angle is geometrically calculated :

$$\varphi = \arctan\left(\frac{\tan \Delta\gamma}{\cos \Delta\beta}\right) \quad (24)$$

In the figure that follows the flow velocity components normal to the hole surfaces on the yaw plane are laying.

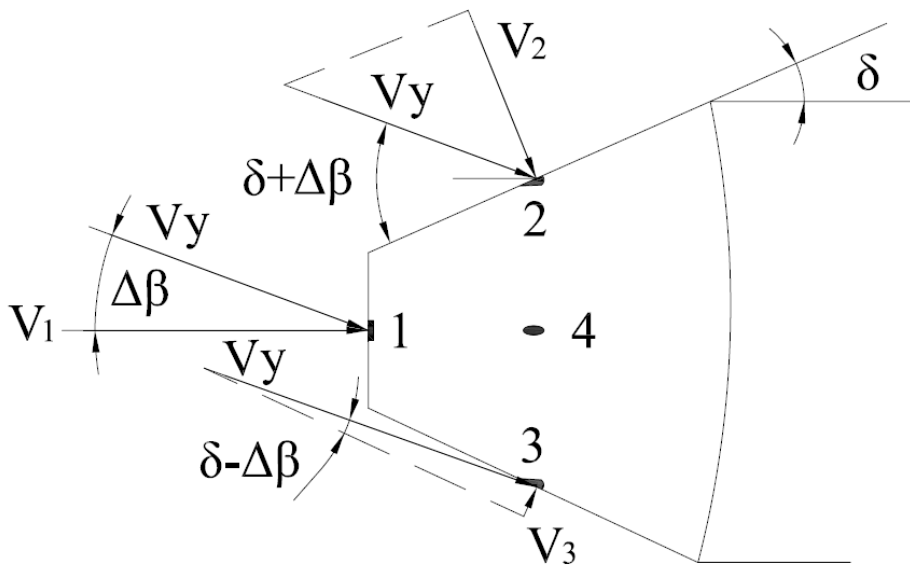


Figure 13: Flow velocity components on the yaw plane

The flow velocity components are:

$$V_1 = V_y \cdot \cos \Delta\beta = V \cdot \cos \Delta\gamma \cdot \cos \Delta\beta \quad (25)$$

$$V_2 = V_y \cdot \sin(\delta + \Delta\beta) = V \cdot \cos \Delta\gamma \cdot \sin(\delta + \Delta\beta) \quad (26)$$

$$V_3 = V_y \cdot \sin(\delta - \Delta\beta) = V \cdot \cos \Delta\gamma \cdot \sin(\delta - \Delta\beta) \quad (27)$$

The flow velocity components for the pitch plane are shown below (Fig 14)

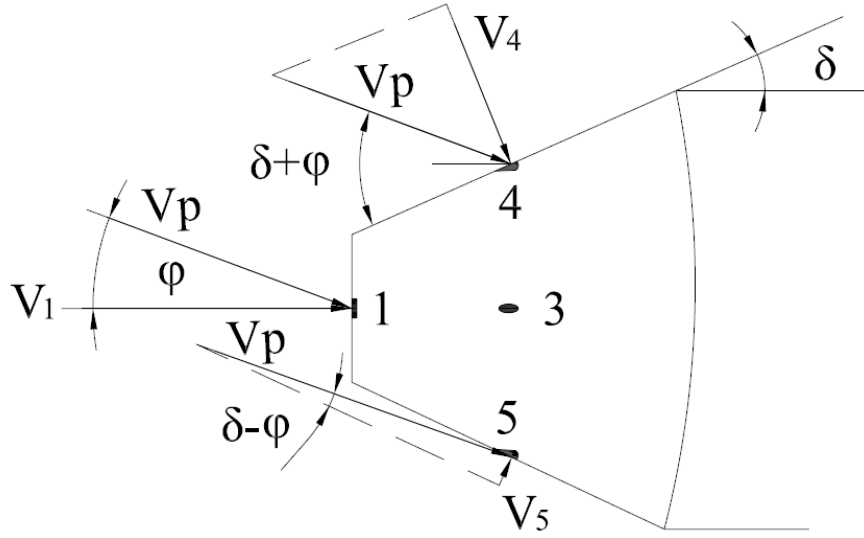


Figure 14: Flow velocity components on the pitch plane

The obtained flow velocity components are:

$$V_4 = V_p \cdot \sin(\delta + \varphi) = V \cdot \frac{\cos \Delta\beta \cdot \cos \Delta\gamma}{\cos \varphi} \cdot \sin(\delta + \varphi) \quad (28)$$

$$V_5 = V_p \cdot \sin(\delta - \varphi) = V \cdot \frac{\cos \Delta\beta \cdot \cos \Delta\gamma}{\cos \varphi} \cdot \sin(\delta - \varphi) \quad (29)$$

Under the assumption of the streamline projection method, and as it follows from Eq. (19), the pressures sensed by the five holes are:

$$p_1 = p + \frac{1}{2} \cdot \rho \cdot (V \cdot \cos \Delta\gamma \cdot \cos \Delta\beta)^2 \quad (30)$$

$$p_2 = p + \frac{1}{2} \cdot \rho \cdot (V \cdot \cos \Delta\gamma \cdot \sin(\delta + \Delta\beta))^2 \quad (31)$$

$$p_3 = p + \frac{1}{2} \cdot \rho \cdot (V \cdot \cos \Delta\gamma \cdot \sin(\delta - \Delta\beta))^2 \quad (32)$$

$$p_4 = p + \frac{1}{2} \cdot \rho \cdot \left(V \cdot \frac{\cos \Delta\beta \cdot \cos \Delta\gamma}{\cos \varphi} \cdot \sin(\delta + \varphi) \right)^2 \quad (33)$$

$$p_5 = p + \frac{1}{2} \cdot \rho \cdot \left(V \cdot \frac{\cos \Delta\beta \cdot \cos \Delta\gamma}{\cos \varphi} \cdot \sin(\delta - \varphi) \right)^2 \quad (34)$$

Hole coefficients:

The hole coefficients are obtained from Eq. (21)

$$k_1 = (\cos \Delta\gamma \cdot \cos \Delta\beta)^2 \quad (35)$$

$$k_2 = (\cos \Delta\gamma \cdot \sin(\delta + \Delta\beta))^2 \quad (36)$$

$$k_3 = (\cos \Delta\gamma \cdot \sin(\delta + \Delta\beta))^2 \quad (37)$$

$$k_4 = \left(\frac{\cos \Delta\beta \cdot \cos \Delta\gamma}{\cos \varphi} \cdot \sin(\delta + \varphi) \right)^2 \quad (38)$$

$$k_5 = \left(\frac{\cos \Delta\beta \cdot \cos \Delta\gamma}{\cos \varphi} \cdot \sin(\delta - \varphi) \right)^2 \quad (39)$$

It should be noticed that the hole coefficient k_1 only depends on the flow attack angles. On the other hand, the hole coefficients k_2 , k_3 , k_4 , and k_5 are functions of the yaw and pitch angles as well as the wedge angle.

The corresponding calibration coefficients can be obtained from its own theoretical definition. See Eqs. (9) to (12).

Direction coefficients:

$$k_\beta = \frac{p_2 - p_3}{p_1 - \bar{p}} = \frac{[\cos \Delta\gamma]^2 \cdot [\sin(\delta + \Delta\beta) - \sin(\delta - \Delta\beta)]^2}{(\cos \Delta\beta \cdot \cos \Delta\gamma)^2 - \bar{k}} \quad (40)$$

$$k_\gamma = \frac{p_4 - p_5}{p_1 - \bar{p}} = \frac{\left[\frac{\cos \Delta\beta \cdot \cos \Delta\gamma}{\cos \varphi} \right]^2 \cdot [\sin(\delta + \Delta\beta) - \sin(\delta - \Delta\beta)]^2}{(\cos \Delta\beta \cdot \cos \Delta\gamma)^2 - \bar{k}} \quad (41)$$

Total pressure coefficient:

$$k_t = \frac{\bar{p} - p_t}{p_t - \bar{p}} = \frac{(\cos \Delta\beta \cdot \cos \Delta\gamma)^2 - 1}{(\cos \Delta\beta \cdot \cos \Delta\gamma)^2 - \bar{k}} \quad (42)$$

Static pressure coefficient:

$$k_s = \frac{\bar{p} - p}{p_t - \bar{p}} = \frac{\bar{k}}{k_1 - \bar{k}} = \frac{\bar{k}}{(\cos \Delta\gamma \cdot \cos \Delta\beta)^2 - \bar{k}} \quad (43)$$

where:

$$\bar{k} = \frac{k_2 + k_3 + k_4 + k_5}{4} = \frac{1}{4} \left[\begin{aligned} & [\cos \Delta\gamma \cdot \sin(\delta + \Delta\beta)]^2 + [\cos \Delta\gamma \cdot \sin(\delta - \Delta\beta)]^2 + \\ & \left[\frac{\cos \Delta\beta \cdot \cos \Delta\gamma}{\cos \varphi} \cdot \sin(\delta + \varphi) \right]^2 + \left[\frac{\cos \Delta\beta \cdot \cos \Delta\gamma}{\cos \varphi} \cdot \sin(\delta - \varphi) \right]^2 \end{aligned} \right]$$

4.2. Prismatic shaped probes

As mentioned earlier, the prism shaped pressure probes have complex head geometry which in turn doesn't allow the theoretical estimation of the probes' calibration coefficients with the streamline projection method.

5. Test Facility

Due to the fact that the flow velocity and flow direction cannot be measured directly by the probes as well as due to some inaccuracies when manufacturing the probe's head, a calibration process is necessary. For this purpose there is the need of a wind tunnel giving flow conditions well known and constant. Problems often concern the flow quality, some geometric restrictions when introducing different probes, and others.

The experimental data for the probes calibration were acquired in the free jet wind tunnel of the Institute of Thermodynamics and Energy Conversion at the Vienna University of Technology.

The five-hole pressure probes employed in this study are used in a fixed position or non-nulling mode. This means that relationships must be determined between the measured pressures at the five holes and the true, total and static pressure or velocity. These desired relationships are usually expressed as dimensionless pressure coefficients, which are functions of the flow angularity. Since, when in use, the flow angles are unknown, relationships between the five measured pressures and the flow direction are also required.

5.1. Description of the wind tunnel

A 50 kW DC motor powers the wind tunnel, with transmission for speed control. The motor drives a radial blower that is 1115 mm in diameter, and it supplies 10.800 m³/h airflow.

The motor-and-blower assembly is mounted on a concrete base and it is isolated from the diffuser. The diffuser divergence angle is about 5,7°. The wind tunnel is equipped with nylon screens, which are used upstream of the nozzle inlet, to serve for a homogeneous flow field at a low level of turbulence. The stream wise turbulence intensity is about 1%. A single hot-wire probe DANTEC 55P11 was used to measure it.

The wind tunnel is provided with 8 pressure sensors and a temperature sensor as well.

The free jet discharges out through a conventional atmospheric exit. The throat diameter of the converging nozzle is $d_n = 120\text{ mm}$, and since the settling chamber diameter is 1000 mm , the convergent contraction ratio is about 1:69,4.

A summary of the free jet wind tunnel technical characteristics can be found in Table 1, while Fig. 15 shows a sketch of the free jet wind tunnel.

| | |
|----------------------|-------------------------|
| Nozzle diameter | 120 mm |
| Contraction ratio | 1: 69,4 |
| Diffuser divergence | 5,7° |
| Turbulence intensity | 1% |
| Total temperature | $\approx 293\text{ K}$ |
| Mach number | 0,05 – 0,3 |
| Reynolds number | Depending on Ma |
| Installed power | 50 kW DC motor |
| Volume flow rate | $3\text{ m}^3/\text{s}$ |

Table 1: Main data of the wind tunnel

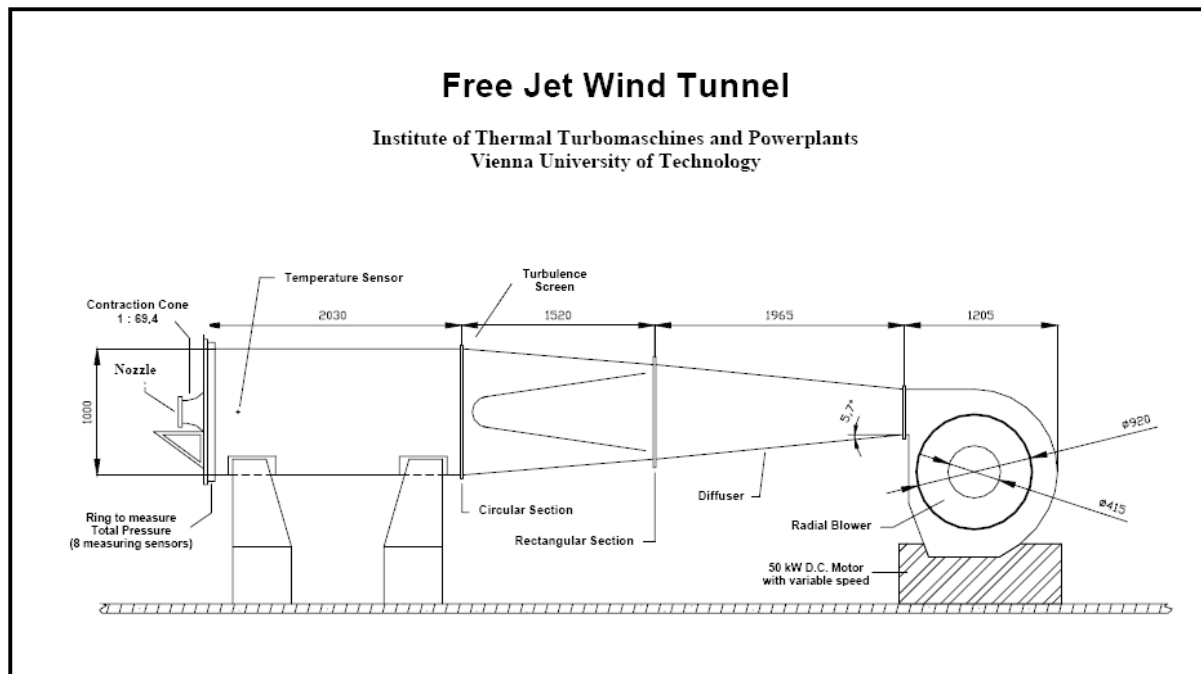


Figure 15: Vienna University of Technology free jet wind tunnel

5.2. Experimental calibration

The three-hole pressure probes calibration is done within a Mach number range ($0,09 \leq Ma \leq 0,19$), at different Reynolds numbers as well as considering an interval of flow angles. Since the experimental measurements are carried out in a free jet discharging to the atmosphere, the Reynolds number is directly linked to the Mach number.

Calibration of these probes are often carried out in an open jet wind tunnel because of the large blockage errors [11] that occur when the calibration set up is placed in a closed wind tunnel test section. The air quality, in terms of low turbulence and uniformity of flow in a closed test section is, however, superior to that of an open jet.

It is known that measurements of the total and the static pressures in the free jet downstream of the nozzle exit prove the existence of a homogenous flow field in the range:

$$0 \leq x \leq 2,5 \times d_n$$

where the variable x represents the distance downstream from the nozzle exit plane to the probe tip location. Outside this core regime, the local total pressure rapidly decreases down to 75% of its value in the settling chamber [2]. So when $x \approx d_n$, it is accepted that the flow characteristics - speed, turbulence, pressure, etc... - are the most convenient to measure the desired values. Thus, the probe is mounted in a support device (see Fig. 16), and it is placed $x=130\text{mm}$ downstream.

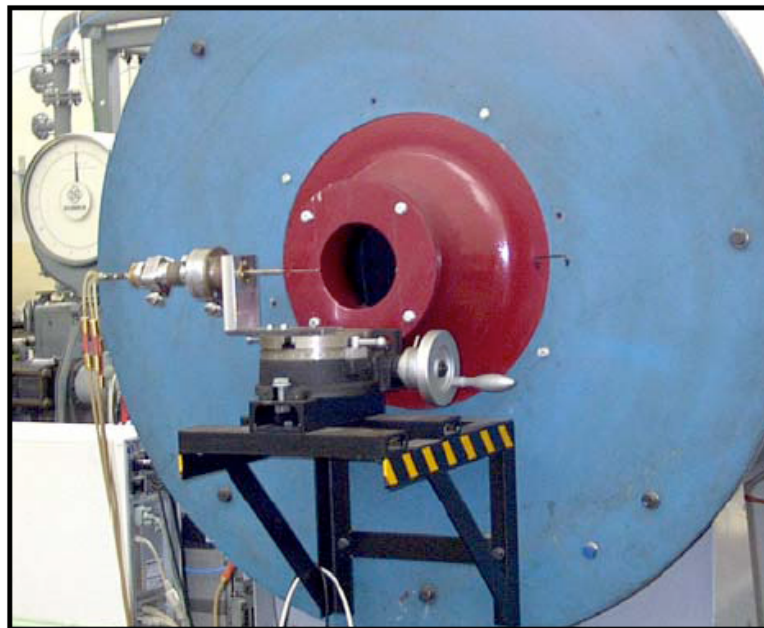


Figure 16: Support device and probe location

On the other hand, the probe tip was located four support diameters upstream of this member to avoid support interference effects. The support was extended four support diameters beyond the tubing to improve the flow symmetry at the probe tip.

The previously discussed device permits a rotation of the probe around the shaft and the perpendicular axis (change in yaw angle $\Delta\beta$ and pitch angle $\Delta\gamma$), so the probe's orientation can be varied from -30° up to $+30^\circ$ in both planes. Even though the rotation of the probe is manual, angles are adjusted in steps of 5° in yaw and pitch respectively with an absolute accuracy of about $0,1^\circ$.

During the calibrations, precautions are taken to insure that the probes are located in the potential core of the jet. The assembly keeps the probe tip at the centerline for all movements. In each case, the probe head blockage ranges between 1,6% and 3,0% of the nozzle exit area.

$$B\% = \frac{A_p}{A_n} \cdot 100 \quad (44)$$

where:

B = total blockage
 A_p = probe head blockage area
 A_n = nozzle exit area

At each calibration point, the five-hole probe provides five pressure measurements. These pressure signals are converted into electrical signals through piezoresistive pressure transducers (HONEYWELL). These transducers are commonly used to simplify the measurement of the pressure from a multi-tube probe (such as a five-hole probe).

Primarily, pressure transducers consist of either flexible diaphragms or piezoelectric elements [3]. The piezoelectric transducer has as its element a crystalline substance that generates an electric field as it is mechanically deformed. The crystal is shaped as a cylinder, wafer or bar; it is generally plated on opposite surfaces, and the electric charge is generated across those plates. The voltage is proportional to the force applied and therefore to the pressure difference.

The free stream total pressure p_t and the stagnation point pressure p_1 are measured using two identical piezoresistive transducers. In this case, the range of work for the measuring instrument is from 0 up to $+138 \text{ mbar}$

The outer hole pressures $p_2, p_3, p_4,$ and p_5 are measured using a single transducer by means of a scanning box (FURNESS CONTROLS). This device allows the use of the same output channel in order to minimize any errors arising

from the transducer calibration. Since these pressures are relative to the atmospheric one, they can be positive, but also negative. Thus, a differential piezoresistive transducer is needed. Its range of work is from -69 up to $+69\text{ mbar}$.

All piezoresistive pressure transducers are powered with 8V DC . The voltage is measured by the HP 44702B 13-bit high-speed voltmeter.

The reference total pressure is measured in the upstream settling section, and atmospheric pressure is used as a reference static pressure. So the pressures are recorded relative to atmospheric pressure p_{ref} i.e.,

$$\Delta p = p_i - p_{ref} \quad (45)$$

where the subscript i refers to the subject pressure.

A sketch of the complete connections of the hardware and the software related to the data acquisition system is given in Fig. 17.

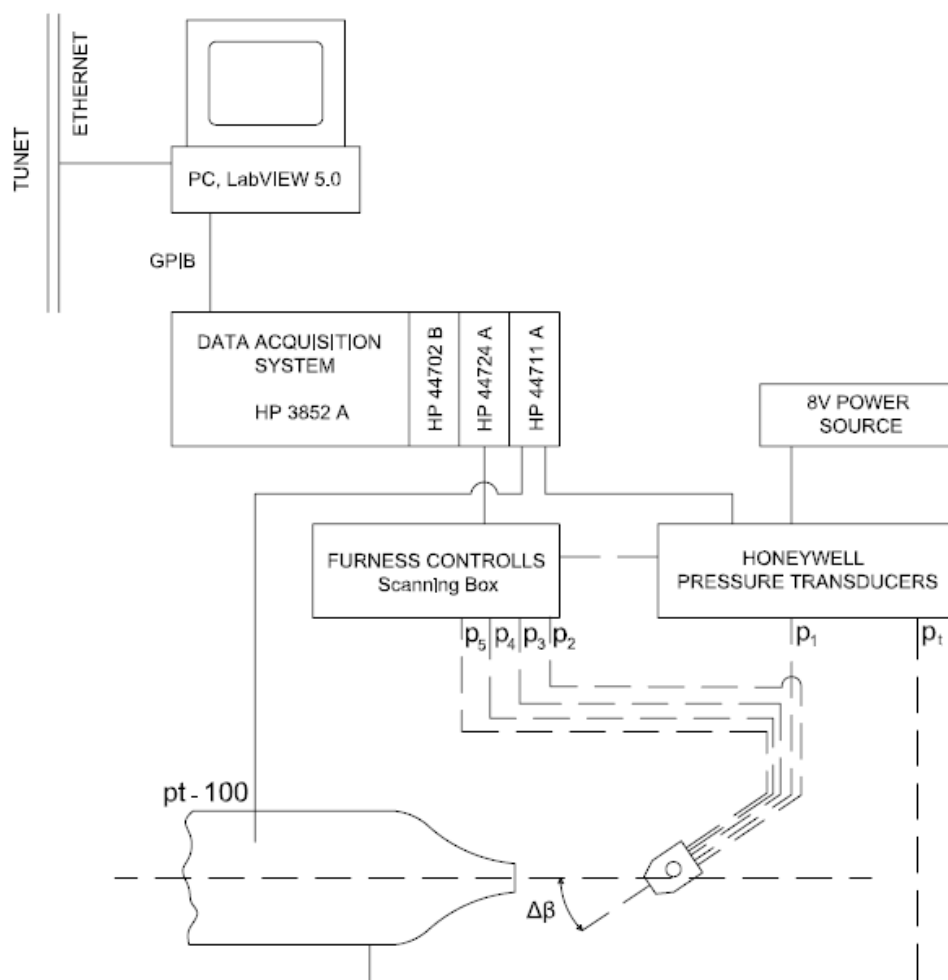


Figure 17: Hardware and software connections for the data acquisition

The flow temperature is measured with a Pt-100 resistor thermometer.

The other components of the data transmission equipment consist of a sixteen-channel HP 44724 A digital output device and a twenty four-channel HP 44711 A multiplexer.

The data recording (taking the relevant wind tunnel data and the probe's readings) is done by the HP 3852 A data acquisition system. It is connected to a PC via the GPIB bus and droved using the LabVIEW software (NATIONAL INSTRUMENTS).

5.3. Flow velocity field

The velocity field section of the wind tunnel and in the potential core of the jet has been shown to be uniform within the accuracy of the experimental measurements by previous studies.

For each probe calibration, the flow velocity is maintained at a constant value. This velocity is adjusted according to the Reynolds numbers Re (based on the jet velocity and probe's head diameter) expected to appear in turbomachines.

In order to guarantee the possibility to compare experimental data and results between the different types of probes, similarity analysis theory [3] is used to keep the relationship between flow velocity field and the probe's head diameter.

“For flow over geometrically similar objects, physical similarity of the velocity fields exists when the Reynolds number is constant. The similarity extends to the dimensionless pressure field.”

In geometry and physically similar situations the flow fields must be similar in all respects, including vortex shedding and the details of the turbulence. It is, however, often difficult (or even impossible) to set up situations that are exactly similar. For example, the surfaces of objects exposed to the flow may be rough. Strict geometric similarity would then require that the roughness elements be similar in shape and distribution. Anyway, when used with proper caution, the similarity relations are a reliable and robust tool.

Thus, it can be concluded that for comparisons, the dimensionless group Re must have the same value. And therefore:

$$Re_1=Re_2 \quad (46)$$

Development of Eq. (46) shows a reverse proportional relationship between flow velocities and the probes' diameters:

$$\frac{d_1}{d_2} = \frac{V_2}{V_1} \quad (47)$$

Taking into account the relationship between the rotational speed n of the fan in the wind tunnel and the velocity V of the fluid, which can be seen in the following function:

$$V = C \cdot n \quad (48)$$

it is easy to see that Eq. (47) can be rewritten as:

$$\frac{d_1}{d_2} = \frac{n_2}{n_1} \quad (49)$$

While calibrating the probes, it is observed that the calibration characteristics can be affected by a variation of the Reynolds number. Hence, the probes are calibrated at various velocities. That is the way to assess the influence of Reynolds number on the experimental data. The calibrations are conducted at $Re=13.000$ and $Re=6.500$, and the rotational velocity of the fan and the velocity of the flow for every test, are summarised in Table 2.

| | | Re=13.000 | | Re=6.500 | |
|--------------------------------|----------------------------|-------------------------------|-----------------------------|-------------------------------|-----------------------------|
| Probe Geometry | d [mm] | n [1/min] | V [m/s] | n [1/min] | V [m/s] |
| conical probe SVUSS/5 | 3 | 1387 | 65,44 | 694 | 32,72 |
| prismatic probe (long) | 3,175 | 1309 | 61.82 | 655 | 30,91 |
| Prismatic probe (short) | 3,175 | 1309 | 61,82 | 655 | 30,91 |

Table 2: Calibration at $Re=13.000$ and $Re=6.500$

The constant C is calculated from Eq (48), if at a random known rotational speed n , the velocity magnitude is calculated from $V = \sqrt{\frac{2}{\rho} \cdot (p_t - p)}$, where p_t and p are known. It is finally obtained that $C=0.0472$, ($V= [m/s]$, $n= [RPM]$)

In fact the calibration was made at 1400 RPM and 700 RPM respectively, because it is not possible to adjust the rotational speed of the blower at the calculated rotational speed. However this deflection from the calculated value is negligible and doesn't affect the results of the experiment.

6. Results and Discussion

A complete set of data is obtained in the laboratory for each one of the five-hole pressure probes. The temperature T of the flow in the free jet wind tunnel and the total pressure p_t as well as the pressures p_i , registered by the five sensing holes, are recorded in an output file at each calibration yaw angle $\Delta\beta$ and pitch angle $\Delta\gamma$, by LabVIEW 5.0.

When introducing the following data:

- atmospheric reference pressure p_{ref}
- environmental temperature T_{ref}
- rotational speed n of the fan
- distance x downstream from the nozzle exit plane to the probe tip location
- characteristic dimension of the probe head d

the data reduction program (written in FORTRAN 77) uses the LabVIEW 5.0 output file as an input file and this enables the procedure to obtain the following information:

- test section flow velocity V
- Mach number Ma
- Reynolds number Re
- hole coefficients k_i
- direction coefficients k_β, k_γ
- total pressure coefficient k_t
- static pressure coefficient k_s

The coefficients mentioned before are then plotted in a 3D contour graph versus the yaw and the pitch angle. The analysis programs which are used nowadays have a high degree of curve-fit accuracy. This yields results with essentially the same value as if the calibration data were used directly in the look up tables, but with reduced errors in the regions of bad calibration points since their effect is reduced by averaging performed by the curve-fitting process. The exact uncertainty of the velocity measurement is a function of not only the curve-fits, which are dependent upon the probe design, but upon the accuracy of the five pressure measurements.

Furthermore, the plots of the hole coefficients as well as the calibration coefficients are also useful when comparing different types of five-hole pressure

probes and when trying to study the effect that changes in the flow conditions produce in the probe's behaviour. For example: the dependency on the Reynolds number, the turbulence intensity influence, errors on the flow angle measurement introduced by a flow velocity gradient, etc...

6.1. Comparison of theoretical and experimental results -Reynolds number and Mach number effects

Meaningful calibration data should be independent of the measured quantities. In most five-hole pressure probes, velocity is the primary parameter to be measured; thus, the effect of changes in Reynolds number Re on the calibration data should be evaluated. The variations are assessed by calibrating the probes in air at different Reynolds numbers: $Re=6.500$ and $Re=13.000$

For compressible flows, except for k_s and k_t , a third calibration coefficient, which is related to a third independent variable, Mach number, is required. The pseudo-Mach number is defined in the following way:

$$\text{Pseudo-Mach number: } k_M = \frac{\bar{P}}{p_1}, \quad (50)$$

but further discussion about this topic is out of scope of this diploma thesis, since the flows researched are incompressible.

In the next section are compared the calibration data obtained in the laboratory at $Re=6.500$ and $Re=13.000$. In the case of the *SVUSS/5 conical* probe, the experimental results are also compared with the theoretical results obtained from the *streamline projection method*.

6.1.1. SVUSS/5 conical probe

Contours of direction coefficient k_β are presented in the next page. In an ideal case each contour should be a straight vertical line [4]. However, actual contours in fig. 18 are far from the ideal ones. In general, the contour at around $\Delta\beta=0^\circ$ approaches the most the ideal one, although it is not vertical. As $|\Delta\beta|$ increases, the contours tend to be curved. This tendency is always found regardless of the Reynolds number. The most noticeable change in k_β at higher Reynolds number is a wavy variation in the $\Delta\gamma$ -direction in the area of $|\Delta\beta| > 15^\circ$. This change is more noticeable at the higher Reynolds number. It is also noted that the absolute values of k_β are higher at $Re=13.000$ than at $Re=6.500$. That interprets in turn that the slope of k_β , which is a measure of the sensitivity of the probe on the flow direction, is getting steeper as increasing the Reynolds number.

Contours of direction coefficient k_γ presented in page 39 show a similar trend to those of k_β . In an ideal case, contours of k_γ should be in the form of a straight horizontal line. Each actual contour on this page is different from that in the ideal case. There are noticeable discrepancies at the lower Reynolds number. At higher Reynolds number the lines are more curved, and have a wavy variation in the $\Delta\beta$ -direction, when $|\Delta\gamma| > 15^\circ$. Along the line of $\Delta\beta = 0^\circ$ the absolute value of k_γ at $Re = 13.000$ is higher than that at $Re = 6.500$. The sensitivity of the probe on the flow direction is also getting higher as increasing the Reynolds number, like the k_β case.

From the theoretical viewpoint the **streamline projection method** approaches relatively well the results of calibration for the calibration coefficients k_β and k_γ . It is also closer to the ideal case since the lines are smooth and symmetrical to the vertical and horizontal axis respectively. On the other hand, phenomena like these produced during the experimental procedure i.e. flow separation, or others like manufacturing irregularities and asymmetries cannot be predicted from a theoretical method.

Contours of static pressure coefficient k_s for two different Reynolds numbers are shown in page 40. The value of k_s lies only in a narrow range of $0 < k_s < 0,5$, in most area except the corners. It is noticeable that there is no symmetry in the contour graphs created from the exported experimental calibration data. The reason for this, might be the probe stem phenomenon or the probe's misalignment on the mounting device. The fact that the central contour line is deformed, is remarkable as well. Moreover, k_s at $Re = 6.500$ has a higher value than that at $Re = 13.000$, due to the Reynolds number effect. Such a conclusion is also reported from Treaster and Yocum [8], Dominy and Hodson [1], and also Lee and Jun [4].

In the case of the static pressure coefficient k_s , the predicted curves from the **streamline projection method** and the experimental results are not in agreement. This coefficient seems to be nearly independent of the flow angle. According to Eq.(12), this disagreement is caused by the "suction side" hole coefficients. "Pressure side" is called the side which is sensing higher pressure per axis, and "suction side" the lower pressure side. Due to the probe head geometry the flow separates at the sharp corner and a large laminar separation is established. The streamline projection method does not take into account any separation on the "suction side" of the probe head and, therefore, it can not model this behaviour.

The effect of the Reynolds number on the total pressure coefficient k_t is introduced in page 41. There are considerable discrepancies which cannot be regarded negligible. In the graphs is also observed the misalignment of the probe axis. However, independent of the Reynolds number, contours of k_t seem to be nearly concentric. It seems that the Reynolds number effect is only noticeable in the area when $|\Delta\beta| \neq 1$ and $|\Delta\gamma| < 20^\circ$, where unexpected contour lines are generate d.

The **streamlined projection method** is a satisfying approach of the measured data for the total pressure coefficient k_t as well. The maximum theoretical value for this coefficient is lower than $k_t = 0$, however there are some measured points that exceed this maximum theoretical value.

It is summarized that for the *SVUSS/5* conical probe, the yaw and the pitch angle coefficients k_β and k_γ respectively, have nearly the same trend as the Reynolds number. The static pressure coefficient k_s is found sensitive to the Reynolds number nearly all over the yaw and pitch angle range. With increasing the Reynolds number, these coefficient values tend to decrease. Finally, it has to be considered that the most Reynolds number sensitive range is located when the flow turns from laminar into turbulent (transition zone). For example, the transition zone for a cylinder shaped body occurs between $Re=2 \times 10^6$ and $Re=6 \times 10^6$ [9]. These values of Reynolds number are far above the range of the available subsonic nozzle design.

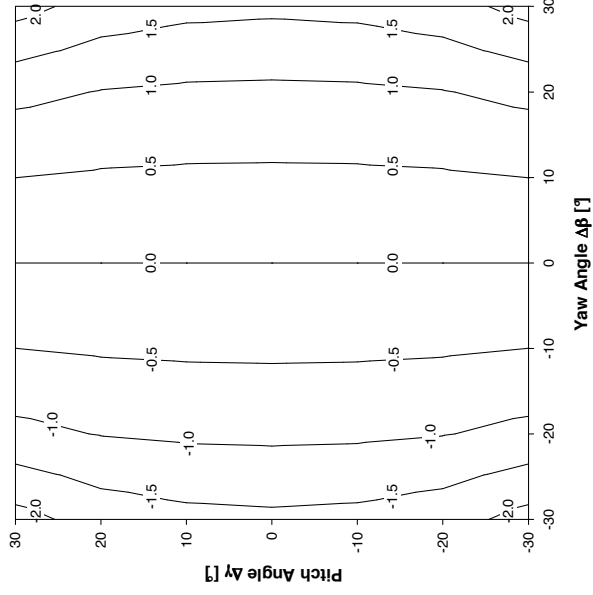


Fig 18(a): streamline projection method

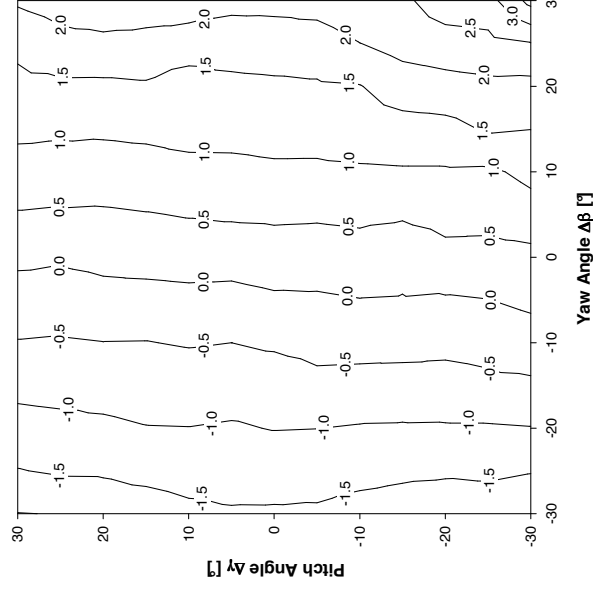


Fig 18(b): experimental calibration at
 $Re=6.500$

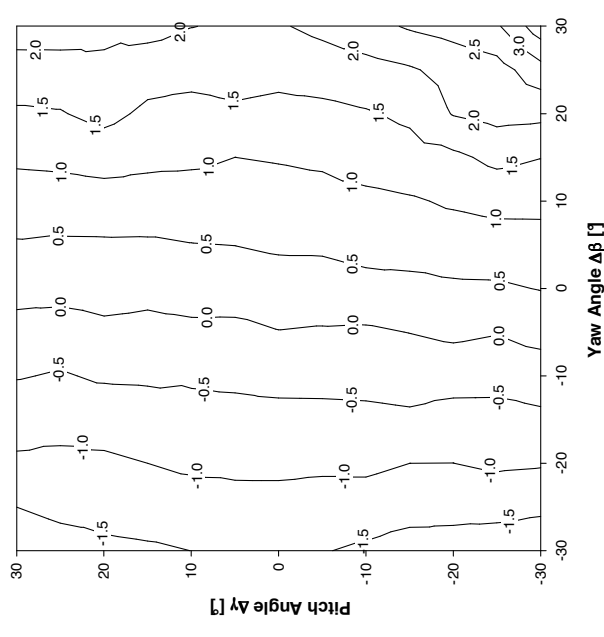
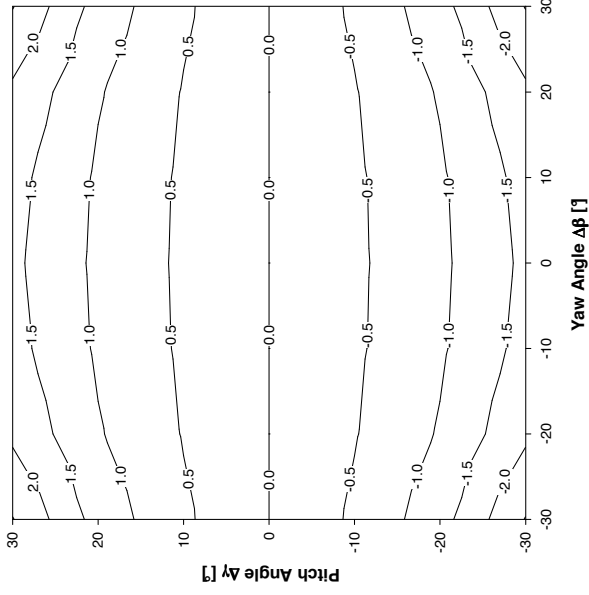
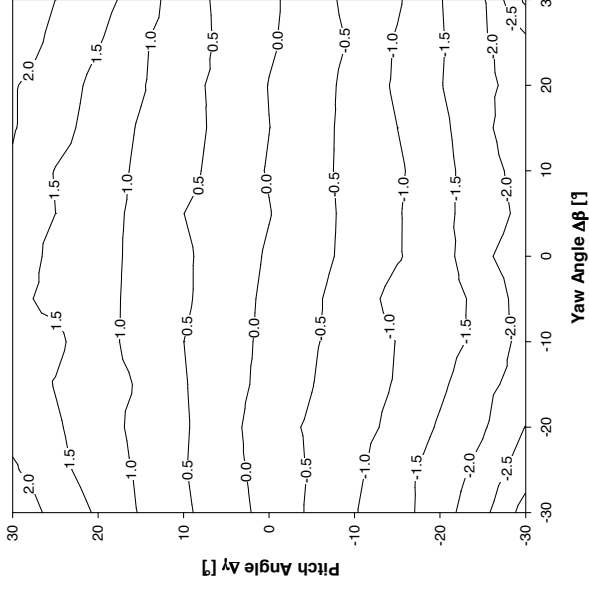
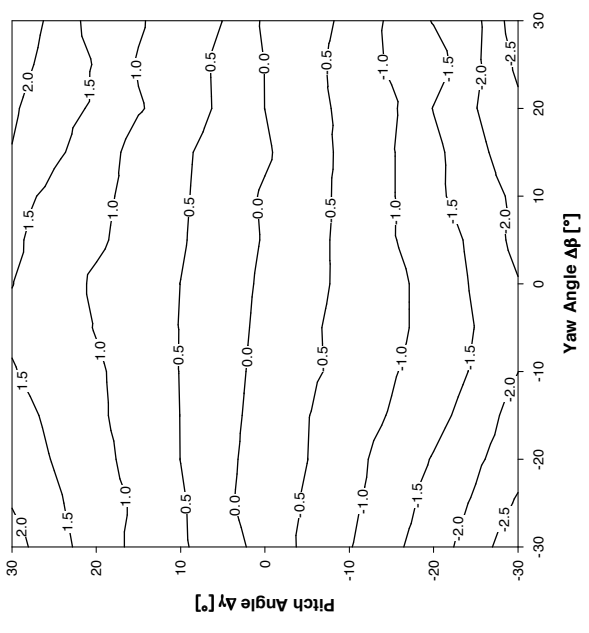
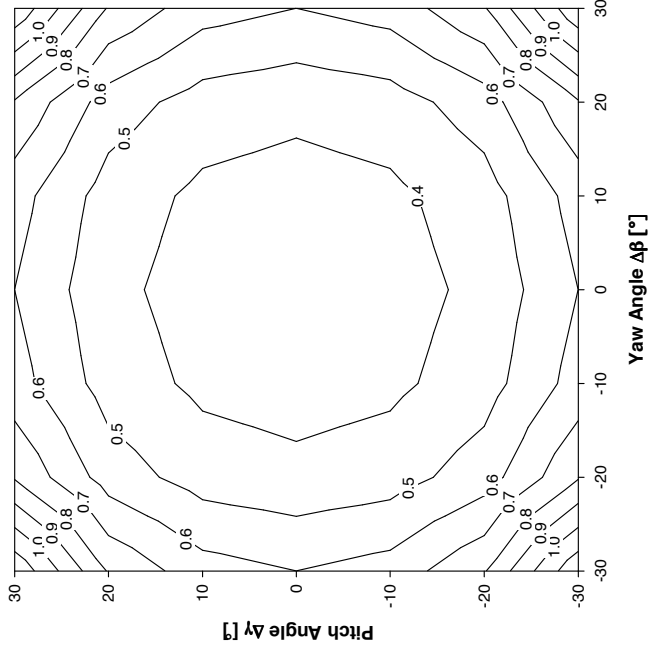
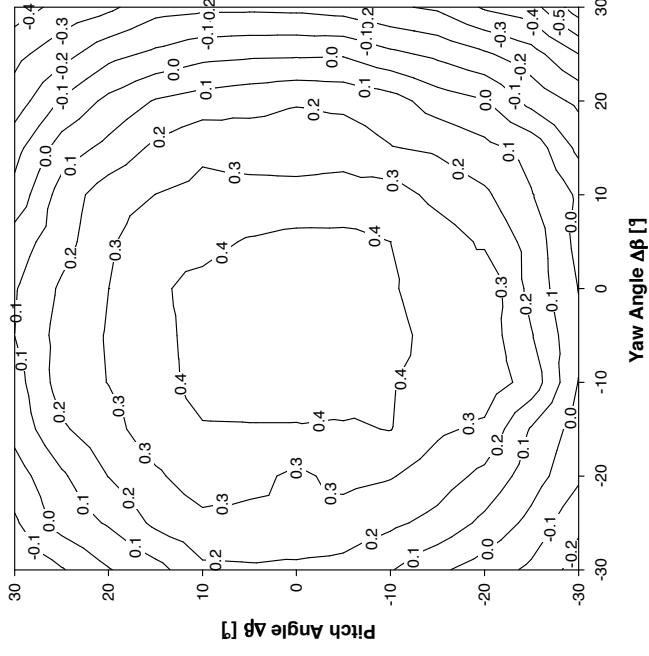
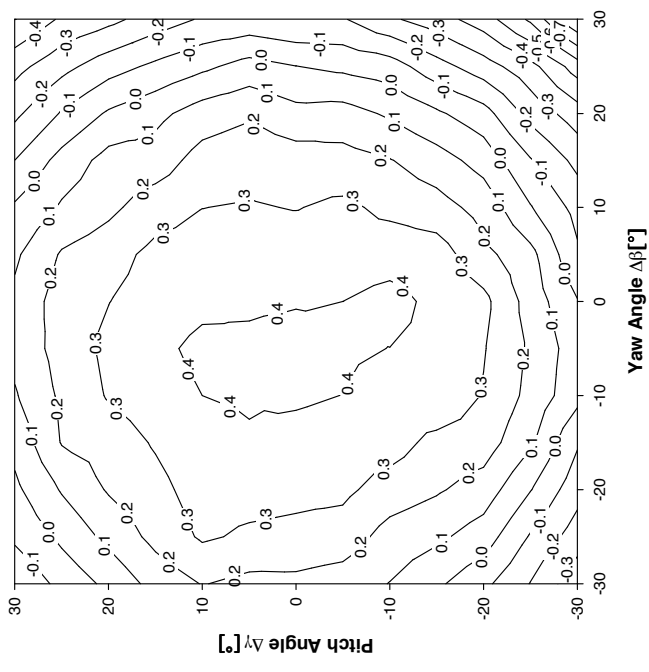


Fig 18(c): experimental calibration at
 $Re=13.000$

Direction coefficient k_β for conical probe

**Fig 19(a):** streamline projection method**Fig 19(b):** experimental calibration at
Re=6.500**Fig 19(c):** experimental calibration at
Re=13.000

Direction coefficient k_y for conical probe

**Fig 20(a):** streamline projection method**Fig 20(b):** experimental calibration at $Re=6.500$ **Fig 20(c):** experimental calibration at $Re=13.000$

Static pressure coefficient k_s for conical probe

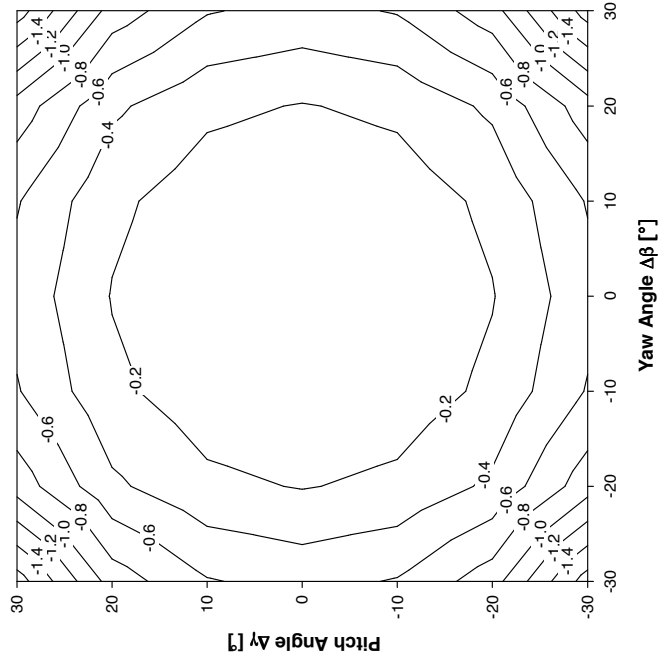


Fig 21(a): streamline projection method

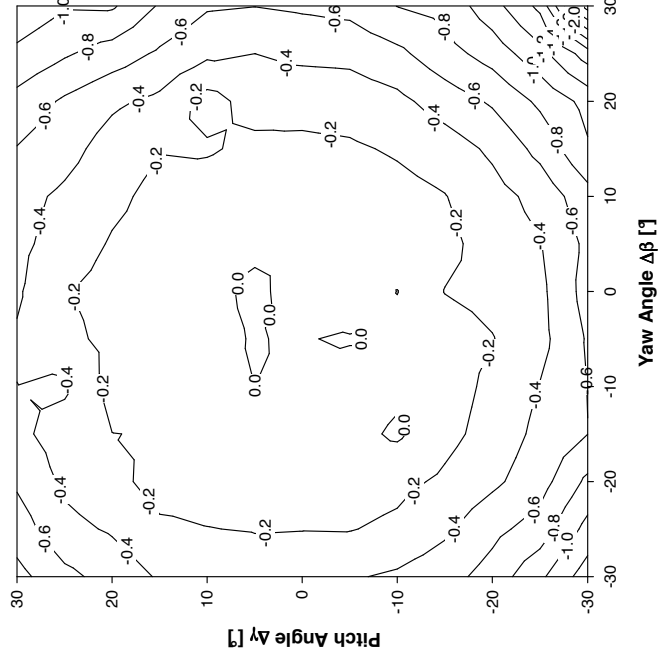


Fig 21(b): experimental calibration at
Re=6.500

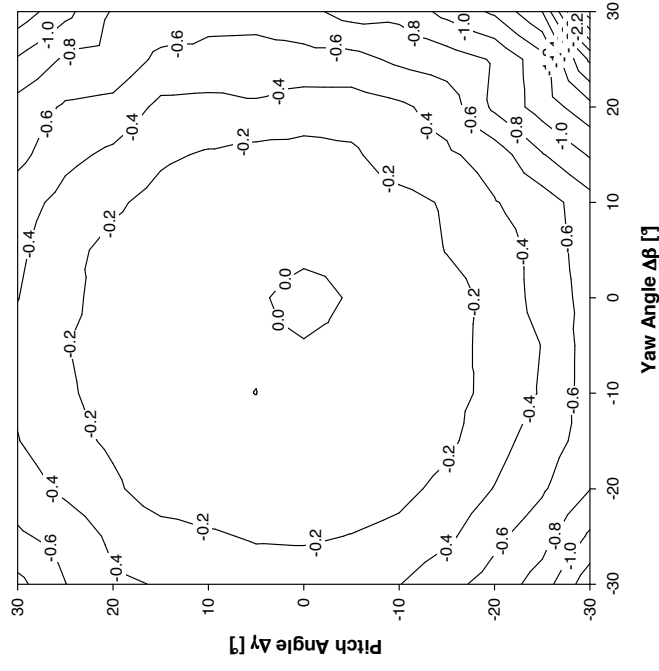


Fig 21(c): experimental calibration at
Re=13.000

Total pressure coefficient k_t for conical probe

6.1.2 Prismatic five-hole probe (*United Sensor*)

The prismatic probe, as mentioned earlier, cannot be modelled by a theoretical method. In the present chapter the behaviour of the probe at $Re=6.500$ and $Re=13.000$ is examined.

The direction coefficients k_β , and k_γ have as expected non-similar behaviour which is explained by the sophisticated head geometry. More precisely the range of values for the k_γ coefficient ($-1,0 \leq k_\gamma \leq 0,8$) is much smaller than that of the k_β ($-4,0 \leq k_\beta \leq 4,0$). The smaller range in k_γ is attributed to the different types of surfaces on which the holes in the two planes are located. This reduced range will result in an increased sensitivity of the prismatic probe to small flow variations in the pitch plane. The velocity component in this plane may, therefore, exhibit more data scatter. On page 44 the contour graphs of k_β coefficient for the two different Reynolds numbers are shown. As can be seen, the changes in Fig 22(a) and 22(b) are imperceptible. After a closer look, it is observed that the values of k_β follow the Reynolds number trend: the higher it is, the higher value range is obtained. That in turn translates into the slope of the curve, which is a measure of the probe's sensitivity on the flow direction, is getting steeper. It is also noted that the contour lines are getting more curved as the Reynolds number increases.

The k_γ coefficient on page 45 has different behaviour from k_β . There are great discrepancies noted, at $Re=6.500$. The contour lines are less curved in comparison with the k_β coefficient. As the Reynolds number increases, these lines tend to become straight horizontal, whilst the discrepancies are smoother. Only the behaviour of the range of values is in agreement with k_β : it is getting a bit larger as the Reynolds numbers increases. The slope is also getting slightly steeper.

At large yaw angles, one hole in the yaw plane is approximately aligned with the flow and senses pressures near the free-stream total pressure. The other hole senses a pressure much less than the free-stream static pressure, due to the acceleration of the flow around the probe and possibly due to flow separation. On the other axis, at large pitch angles, one hole again senses a pressure near the free-stream total pressure, whereas the other hole senses a pressure that is greater than the free stream static pressure. This latter pressure may be higher due to a lower local acceleration and pressure recovery in the separated flow. Thus, the pressure difference sensed by the holes in the yaw plane exceeds the difference measured by the holes in the pitch plane [8]. Taking into account the above, the contour graphs for k_s and k_t for $Re=6.500$ and $Re=13.000$ are examined.

The distribution of the contour lines for the static pressure coefficient k_s is presented on page 46. As can be seen, there is no symmetry and the lines seem randomly set. The reason for this might be the probe stem effect. When increasing the Reynolds number, the similar behaviour of the contour lines remains. The obtained values in this case are a bit different.

On page 47 the contour graphs of the total pressure coefficient k_t for the two Reynolds numbers are presented. The two graphs tend to be symmetrical to the vertical axis for $\Delta\beta=0^\circ$, and in an ideal case the contour lines would be completely

vertical. The range of values at both Reynolds numbers is $-1,0 \leq Re \leq 1,0$ although the maximum value of k_t is higher for $Re=6.500$.

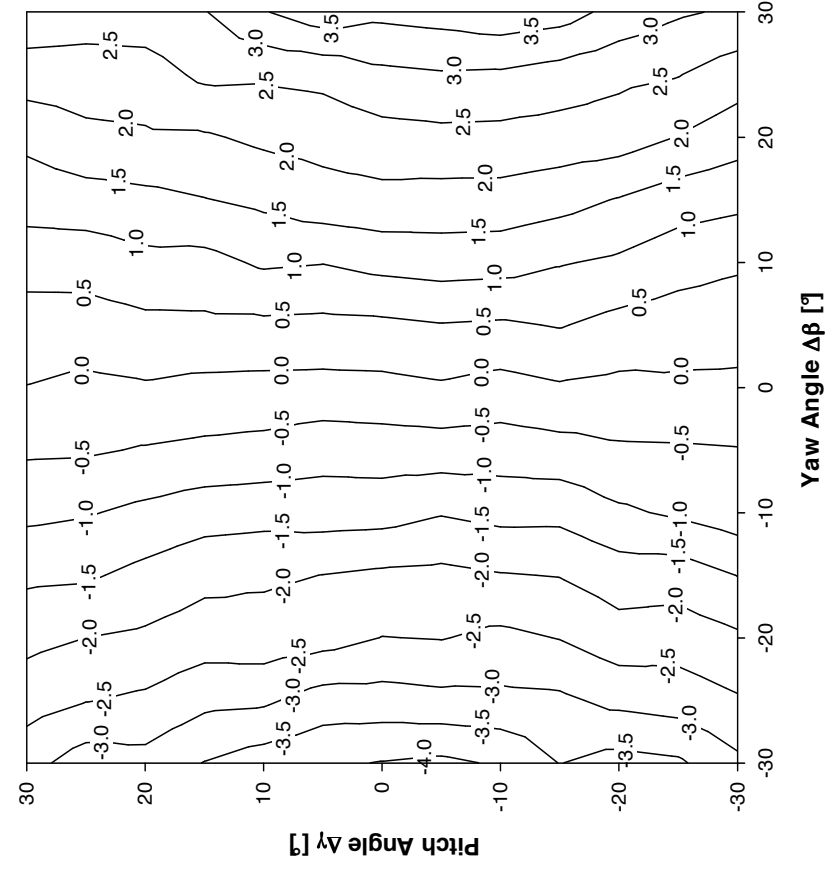


Fig 22(a): experimental calibration at
Re=6.500

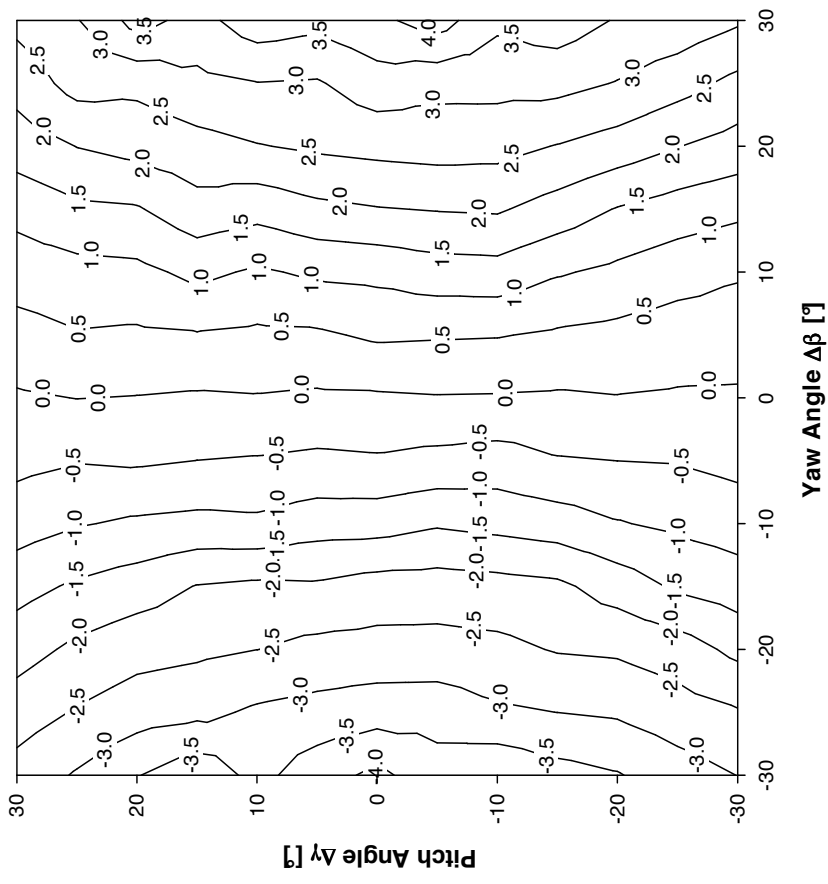


Fig 22(b): experimental calibration at
Re=13.000

Direction coefficient k_β for prismatic long probe

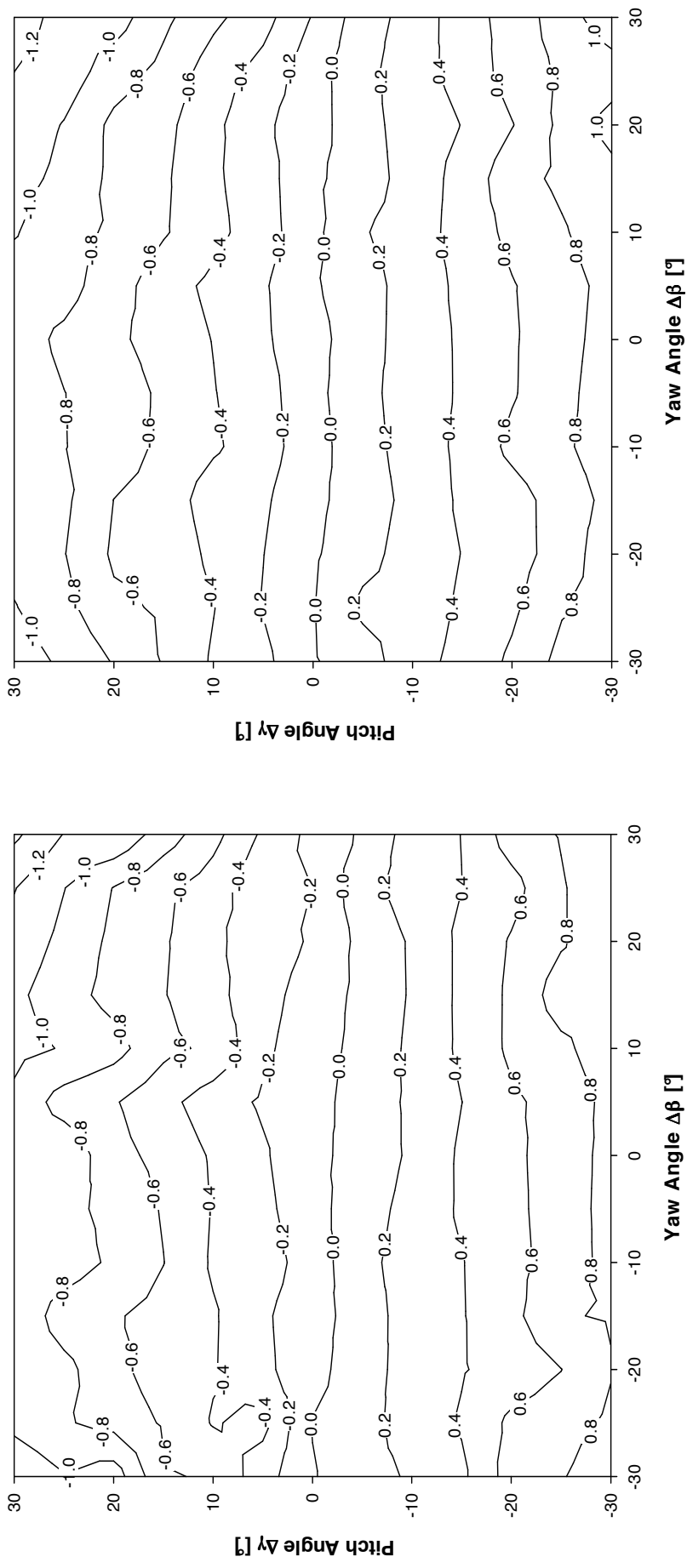


Fig 23(a): experimental calibration at
Re=6.500

Fig 23(b): experimental calibration at
Re=13.000

Direction coefficient k_y for prismatic long probe

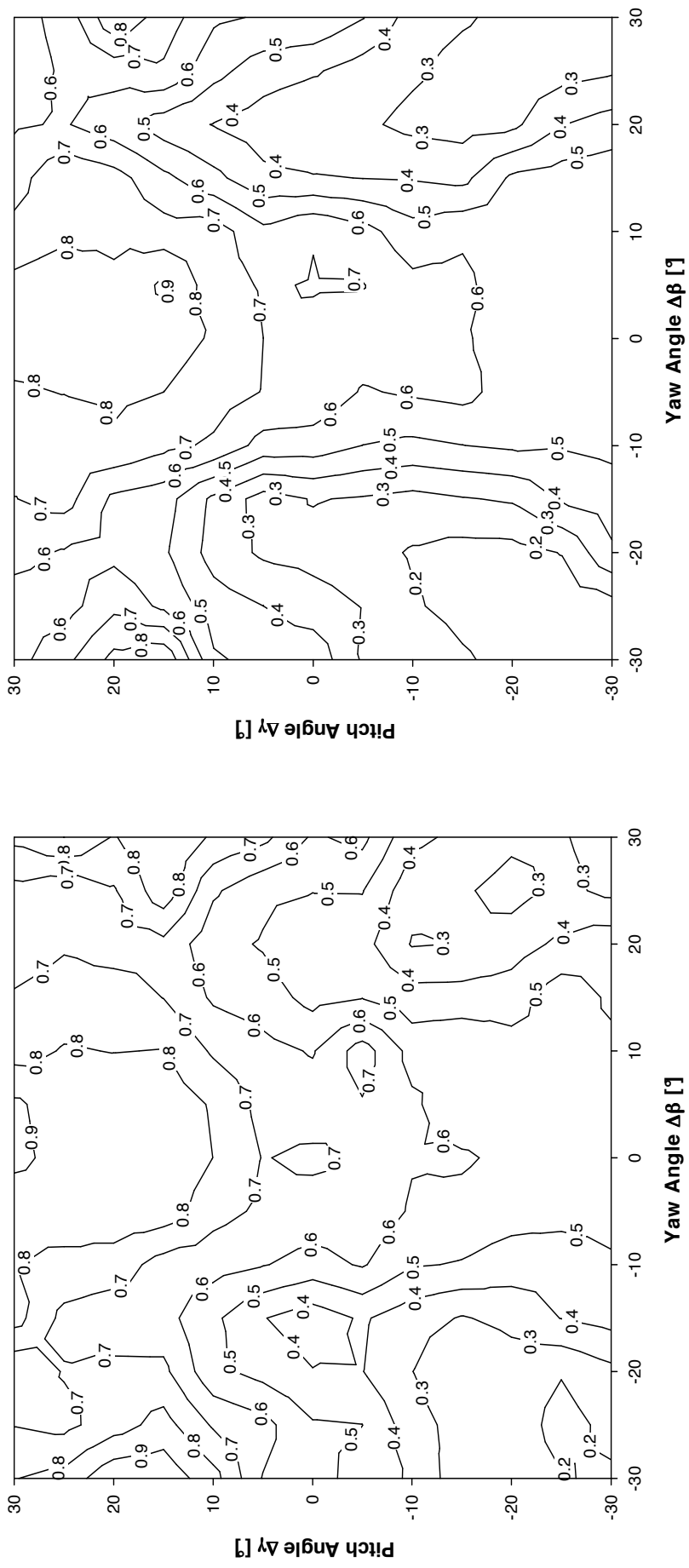


Fig 24(a): experimental calibration at
Re=6.500

Fig 24(b): experimental calibration at
Re=13.000

Static pressure coefficient k_s for prismatic long probe

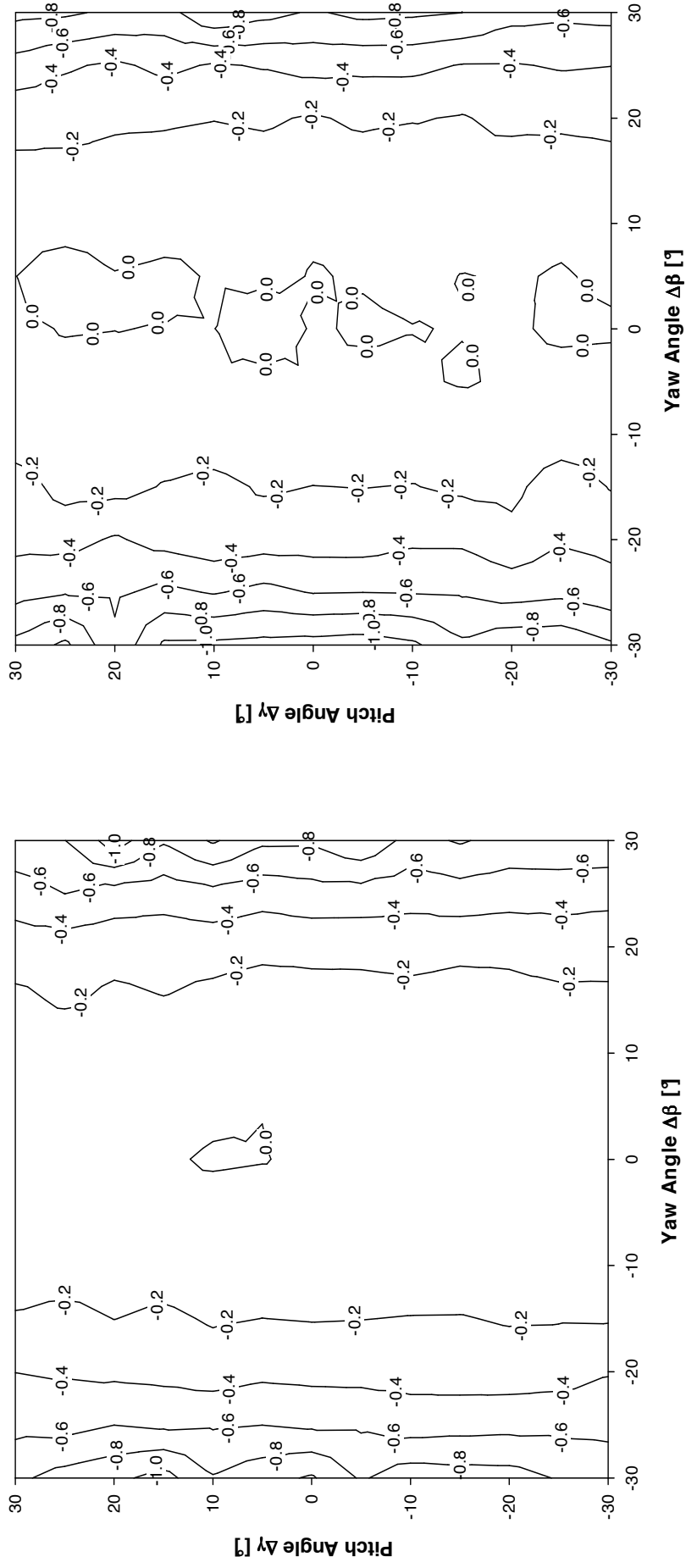


Fig 25(a): experimental calibration at
Re=6.500

Fig 25(b): experimental calibration at
Re=13.000

Total pressure coefficient k_t for prismatic long probe

6.2. Comparison between probes

In the current chapter a comparison between the two commercial prismatic probes manufactured from *United Sensor Corporation* is performed, in order to then be evaluated. The types of the probes are listed below:

- DA-125-24-F-22-C
- DA-125-18-F-16-C

As can be seen from the ordering sheet, the probes have exactly the same head geometry, but different overall lengths. The first is 24" long, while the second is 18".

The four calibration coefficients k_β , k_γ , k_s and k_t obtained at $Re=13.000$ which are used to measure a flow field have been plotted side by side and compared. These plots can also be used to determine the range of flow angles which a particular probe can measure. There is a maximum angle the flow can have with respect to the axis of the probe beyond which the flow separates from the probe. When this occurs the data can not be reduced to obtain the velocity since the pressure taps in the separated region do not vary significantly nor monotonically with flow angle.

On pages 49, 50, 51 and 52 are plotted the k_β , k_γ , k_s and k_t coefficients respectively. The form of the contour lines in page 49 for k_β in both figures are similar. However, the range of values for the short probe is $-3,5 \leq k_\beta \leq 4,5$ while for the long probe is $-4,0 \leq k_\beta \leq 4,0$, fact which demonstrates a possible manufacturing irregularity or misalignment of the probe head.

In the k_γ graphs in page 50 a behaviour that is in disagreement with the ideal case of the straight horizontal lines for the short probe is also noted. The contour lines have a skewed orientation and are curved. The range of values in this case is $-1,4 \leq k_\gamma \leq 1,2$ for the short probe, while $-1,0 \leq k_\gamma \leq 1,0$ for the long probe. The observed conclusions amplify the initial assumption for manufacturing irregularities or misalignment.

For the k_s coefficient on page 51, it is only remarkable that the short probe doesn't have a symmetry axis in contrast with the long probe, which is relatively symmetrical to the $\Delta\beta = 0^\circ$ axis.

The k_t contour graphs on page 52 are quite similar, fact which prevents exporting secure and reliable conclusions.

Summarizing the individual conclusions of each calibration coefficient, it is concluded that the long probe is in better condition. Its behaviour approaches relatively well this one of the ideal probe, and the obtained graphs are similar to these of previous experimental calibrations.

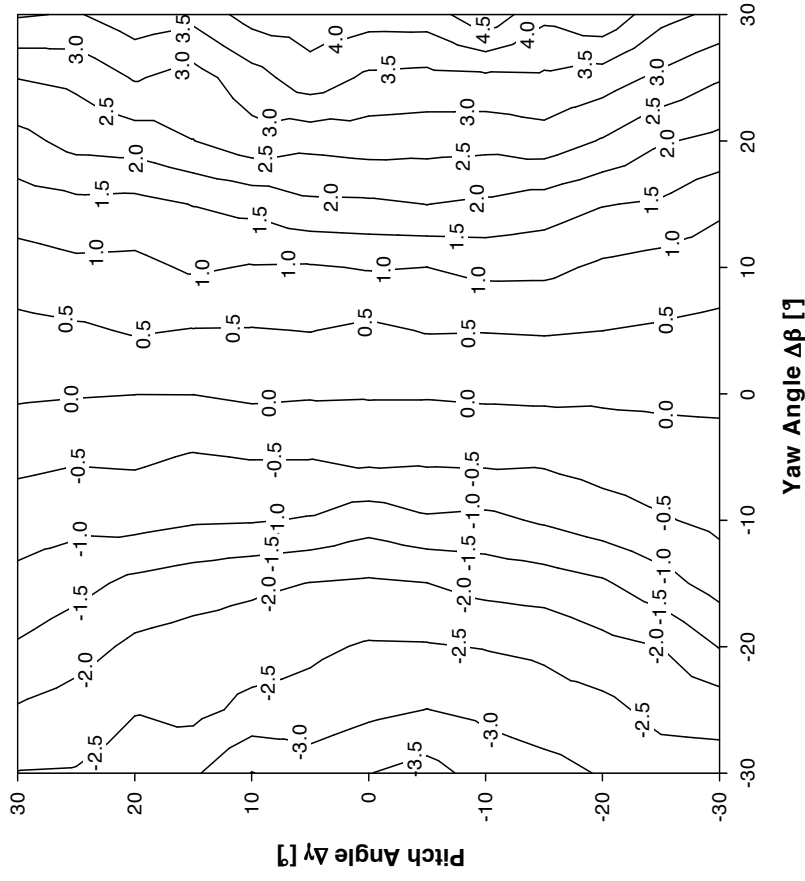


Fig 26(a): experimental calibration at
 $Re=13,000$
 short probe

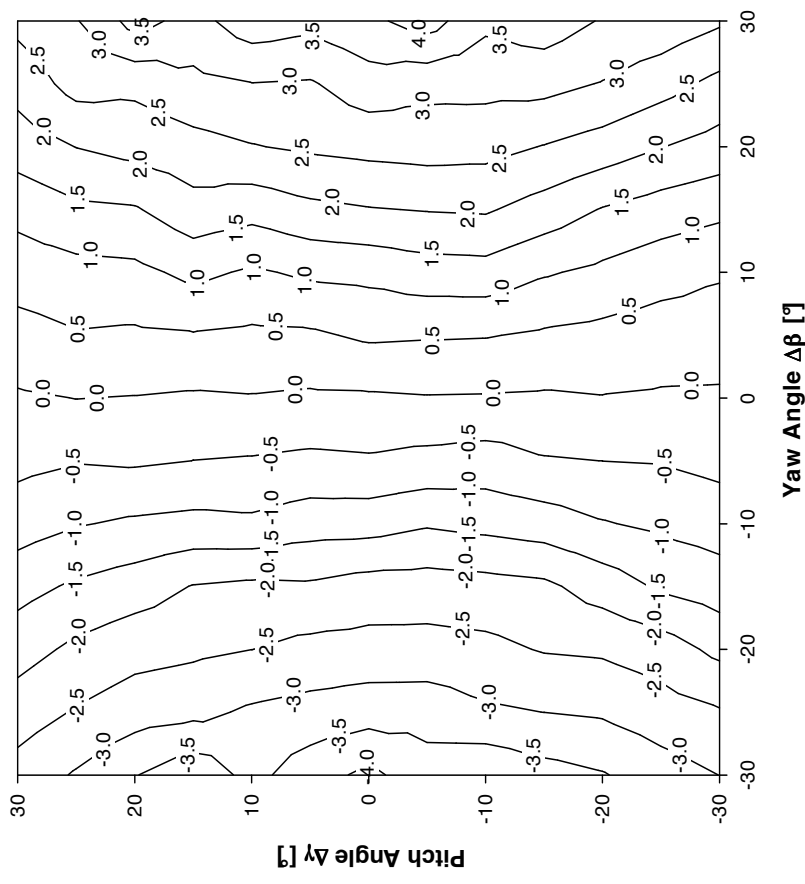


Fig 26(b): experimental calibration at
 $Re=13,000$
 long probe

Direction coefficient k_β for prismatic probe Comparison between short-long probe

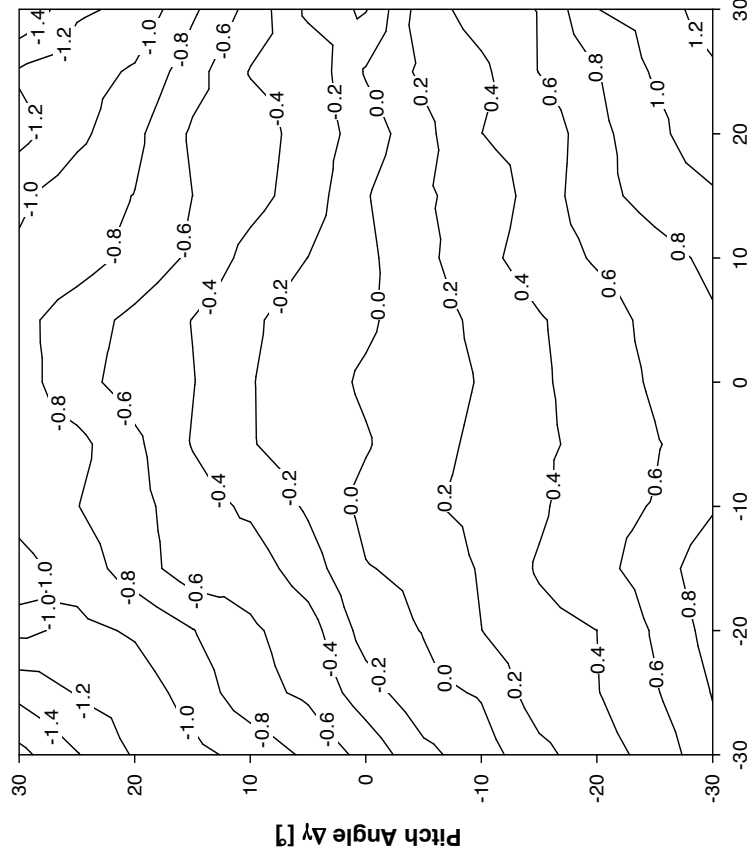


Fig 27(a): experimental calibration at
Re=13.000
short probe

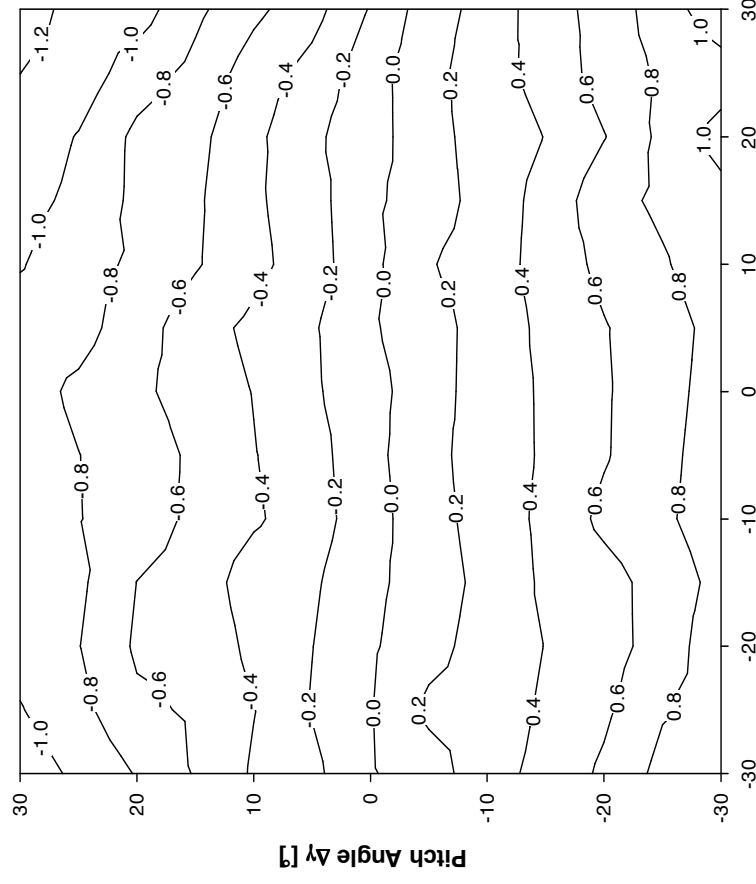


Fig 27(b): experimental calibration at
Re=13.000
long probe

Direction coefficient k_y for prismatic probe Comparison between short-long probe

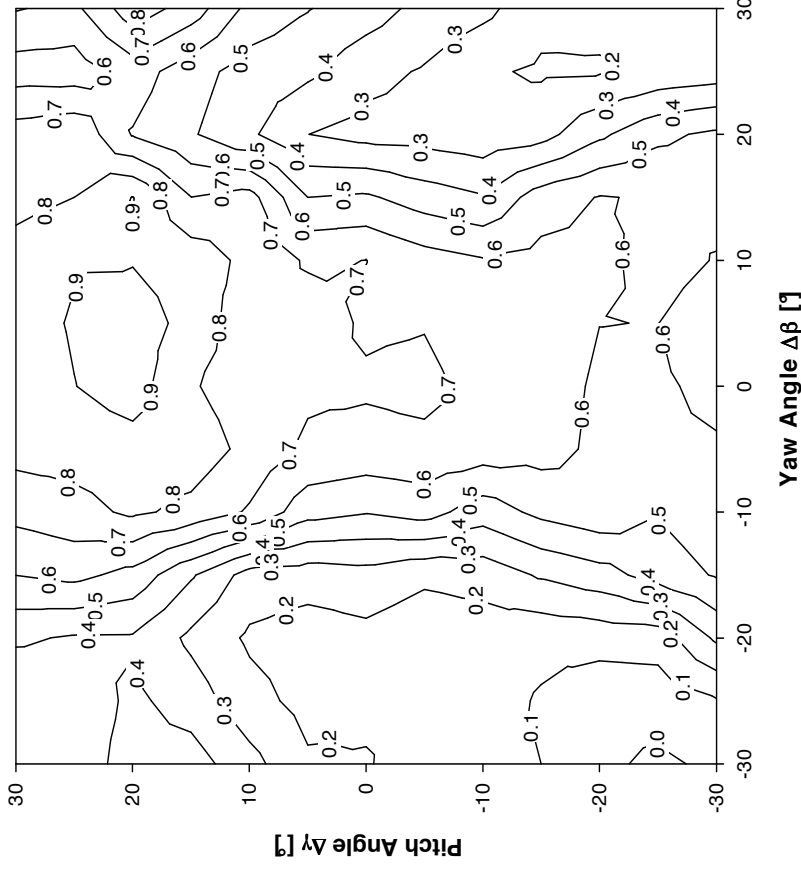


Fig 28(a): experimental calibration at
Re=13.000
 short probe

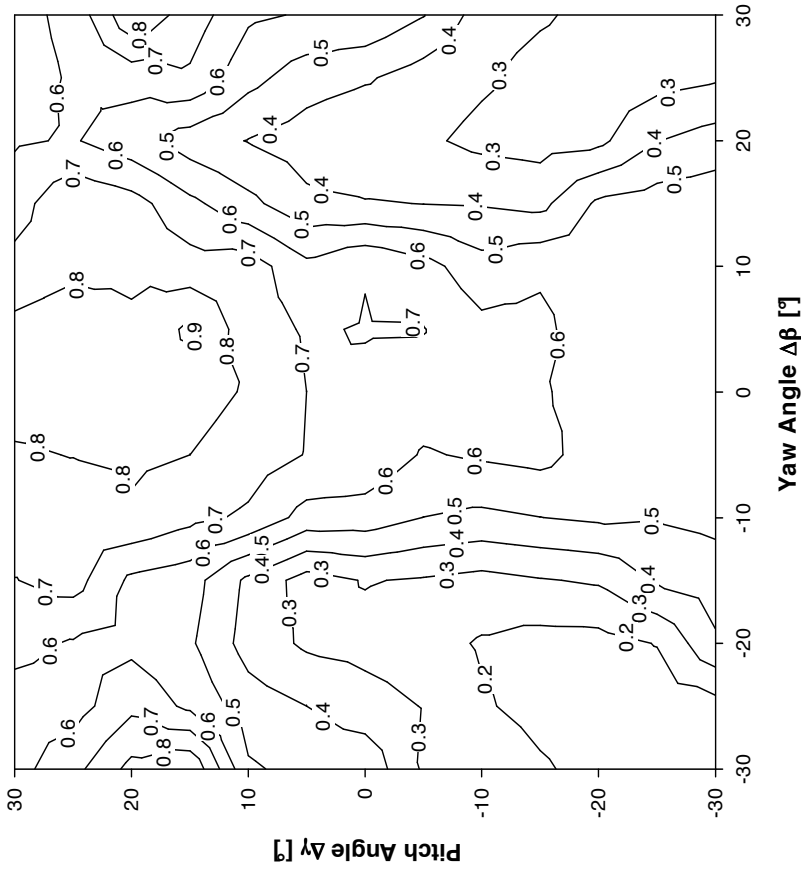


Fig 28(b): experimental calibration at
Re=13.000
 long probe

Static pressure coefficient k_s for cylindrical probe Comparison between short-long probe

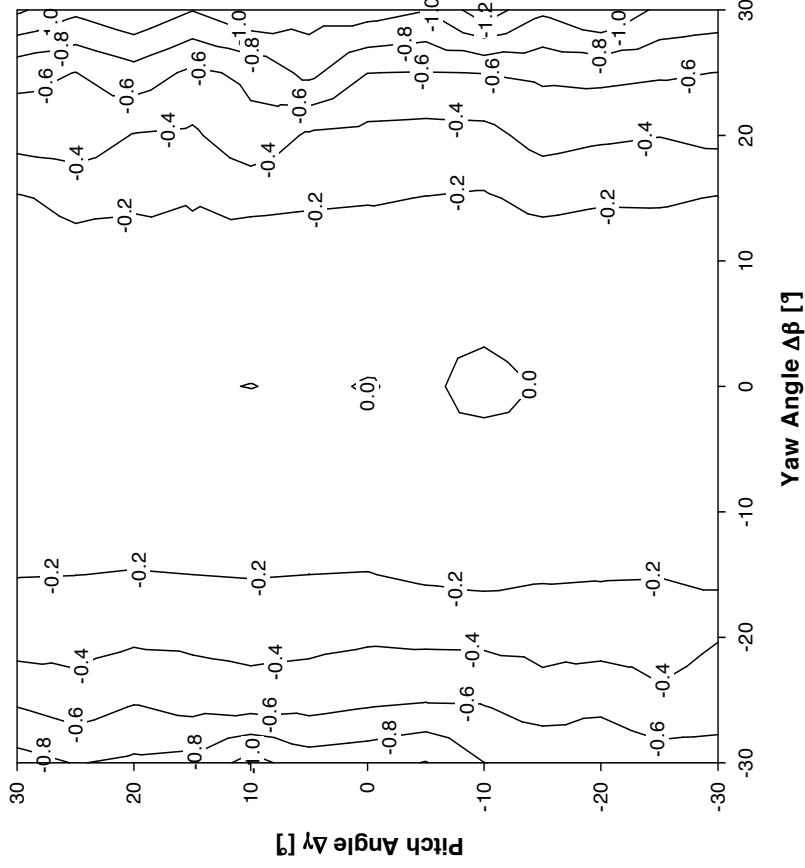


Fig 29(a): experimental calibration at $Re=13,000$ short probe

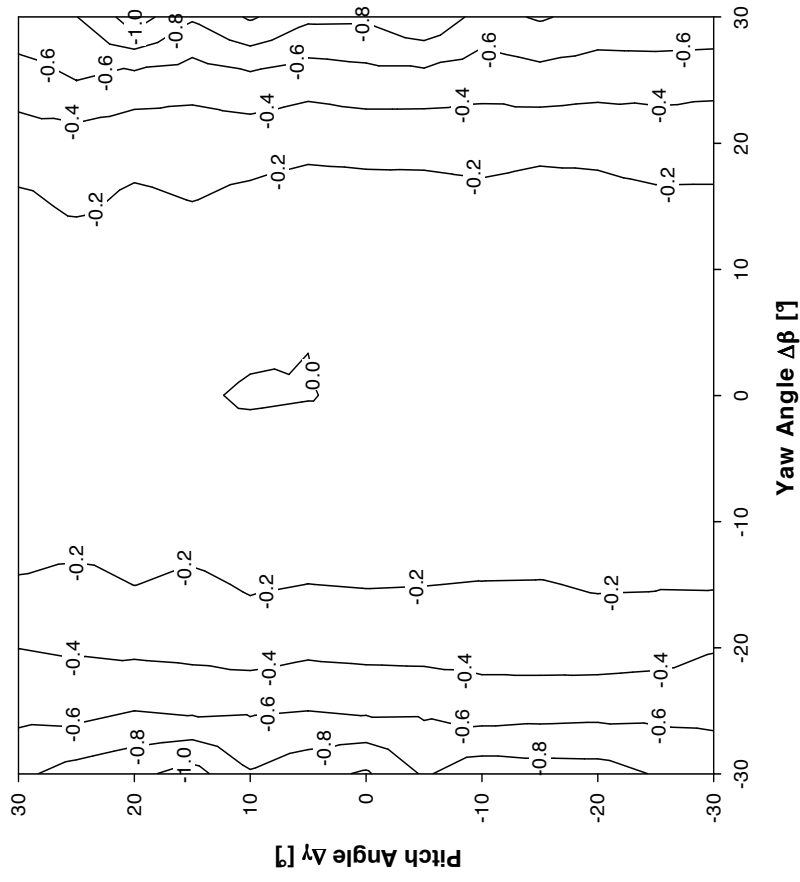


Fig 29(b): experimental calibration at $Re=13,000$ long probe

Total pressure coefficient k_t for prismatic probe Comparison between short-long probe

6.3. Other factors influencing the calibration of five hole probe

The main factors influencing the calibration of a five-hole pressure probe are probe head geometry and Reynolds number. Alignment with the flow direction and manufacturing defects is also significant. The probe head geometry effect and the Reynolds number effect have been discussed at length above. Some other factors, such as: sensing holes geometry, existence of velocity gradients or wall proximity have minor relevance, but they can also affect the behaviour of the probe or introduce sources of error when calibrating or using a pressure probe for flow measurement in turbomachinery.

6.3.1. Hole geometry for static pressure taps [3]

The “ideal” tap geometry is a small circular hole of less than $\frac{1}{4}$ mm diameter drilled perpendicular to the surface on which the pressure is to be measured; the corner of the hole is perfectly sharp and squared off. Any declination of this geometry will introduce error. A 1 mm diameter hole should introduce an error of less than 1% of dynamic pressure, compared with a hole of $\frac{1}{4}$ mm diameter. Errors with practical-sized holes occur because of flow in and around the hole opening. Rounding of the hole corners (up to a radius curvature equal to the hole diameter) and no perpendicularity of the hole with the wall introduce errors of less than 1% of dynamic pressure. Burrs on the edge of the hole, with heights of less than $\frac{1}{30}$ of a hole diameter and extending into the flow, introduce errors of less than 1% of dynamic pressure.

6.3.2. Turbulence intensity

The conventional probes are usually calibrated in a well-controlled calibration tunnel where the flow turbulence is very low. But they are used to measure flow in turbomachinery, where the turbulence fluctuations are large and cause error in pressure probes.

The effect of turbulence is to increase the sensed value of mean static pressure. It is known [3] that the probe static pressure will exceed the true static pressure by an amount of $\frac{1}{4} \cdot \rho \cdot \bar{V}_n^2$, where \bar{V}_n^2 is the resultant turbulence intensity in the circumferential plane of the probe. One can work out that error in the combined $p_t - p$ will be less than in each pressure separately. It may even be negligible, depending on the relative magnitudes of stream wise and transverse intensity components.

Part of the influence of the Reynolds number upon probe calibrations is due to the changing nature of the separations that exist at all flow angles [7]; changes that

stem from the influence that Reynolds numbers exert upon the transition processes within the separation bubbles. Thus, turbulence can affect the reliability of probe calibrations even at typical Reynolds numbers.

6.3.3. Velocity gradient effects [7] [10]

The probes used in this investigation are calibrated in a uniform flow, but they are used to measure flow in turbomachinery components. The flow fields in these conditions are dominated by strong velocity gradients. These gradients affect the probe performance in the following ways:

1. The probe indicates the reading at a location different from the geometric centre of the probe. This perturbation is known as displacement effect.
2. The presence of the probe in a velocity gradient causes deflection of the streamlines toward the region of lower velocity. This deflection causes the probe to indicate pressures in excess of that existing at the same location in the absence of the probe.
3. The velocity gradient induces a pressure difference between the side probe holes, which is interpreted by the probe as a flow angle error $\Delta\epsilon$. Hence, an additional error is introduced.

6.3.4. Wall proximity effects [7]

Whenever a probe is located near a solid surface, the flow acceleration in that region introduces an additional error. In the measurement of flow in a turbomachinery component, the probe is placed close to many solid surfaces, such as annulus wall and blades. A discussion of these errors follows.

When a probe is very near a blade trailing edge, it is subjected to the following effects: viscous and inviscid interference between the probe and the trailing edge, area blockage and velocity and pressure gradients discussed earlier. The complexity of the interaction between the probe and trailing edge prohibits an estimate of the error in the probe measurements, and the results very near the trailing edge should be viewed with caution.

Due to the blockage effect between the probe and the wall, the pressure sensed by the side hole near the wall is higher than the value at the free stream conditions. A rule of thumb is that such interactions cause error when the distance from the axis to the wall is less than two probe diameters. For some of the larger three-hole probes the distance may be more like four diameters. Gradient as well as wall proximity effects are rather difficult to establish in a wind tunnel calibration procedure. Therefore, analytical investigations or CFD computations are an interesting alternative to the wind tunnel calibration.

6.3.5. Influence of probe supports [3]

The pressure gradients associated with the curvature of flow lines around probe supports can be avoided by proper displacement of the probe. For cylindrical probe supports perpendicular to the probe axis, the distance should be five support diameters to avoid an error amounting to 2% of dynamic pressure. For an aerodynamically faired strut, the rule for low Mach numbers might be relaxed to three support diameters.

Endnote I

FORTRAN 77 program

The FORTRAN 77 program used for the data reduction is the following:

```

      program kalib5
c*****Auswertung der Kalibrierung 5-Lochsonde
c
c*****16.11.1999 rwillig:
c      20.06.2000 rwillig: Eingabe Druেকে [mmWS] --> [Pa]
c      23.06.2000 rwillig: 3-Lochsonde --> 5-Lochsonde
c      19.06.2001 rwillig: Erweiterung auf +-30 grad (25 Punkte)
c      27.07.2001 rwillig: Berechnung von Re_min und Re_max
c      22.03.2005 rwillig: n=13 Punkte
c
c*****
c
c*****Variablenvereinbarung:
c
c      character reihe*20
c
c      real kappa, R, tu, pu, dz, x, d, gamma
1      rho, pt, c, Ma, nu, pq, kb, kg, kt, ks, Remin, Remax
c
c      integer i, n
c
c      dimension dbeta(25), t(25), ptpu(25), p1pu(25),
1      p2pu(25), p3pu(25), p4pu(25), p5pu(25),
2      Re(25)
c
c*****Konstantenvereinbarung:
c
c      kappa=1.4
c      R=287.0
c      n=13
c
c*****Oeffnung des Eingabefiles 'kalib5.dat':
c      open (unit=5,file='kalib5.dat')
c
c*****Oeffnung des Text-Ausgabefiles 'kalib5.out':
c      open (unit=6,file='kalib5.out')
c
c*****
c
c*****Ausgabe des Headers:
c
c      call header
c
c*****Nr. der Messreihe:
c
c      read (5,100) reihe
100  format (a10)
c

```

```

        write (6,110) reihe
110   format (6x,'Messreihe Nr.: ',a20,/)
c
c*****Umgebungsbedingungen:
c
        read (5,190) pu, tu
190   format (2f10.0)
c
        write (6,200)
200   format (6x,'Umgebungsbedingungen:')
        write (6,210) pu, tu
210   format (6x,'pu[mbar]   = ',f12.2,3x,'tu[grd]   = ',f12.2,/)
c
        pu=pu*100.0
c
c*****Drehzahl, Duesenabstand, Sondendurchmesser, Nickwinkel:
c
        read (5,230) dz, x, d, gamma
230   format (4f10.0)
c
        write (6,240)
240   format (6x,'Drehzahl, Duesenabst.,Sondendurchm., Nickwinkel:')
        write (6,250) dz, gamma
250   format (6x,'n[U/min]   = ',f12.2,3x,'gamma[grd]= ',f12.3)
        write (6,260) x, d
260   format (6x,'x[mm]     = ',f12.2,3x,'d[mm]     = ',f12.3,/)
c
c*****Einlesen der Messwerte:
c
        do 350 i=1, n
            dbeta(i) = 5.0*i-35.0
            read (5,340) t(i), ptpu(i), p1pu(i), p2pu(i), p3pu(i),
1          p4pu(i), p5pu(i)
340   format (7f10.1)
350   continue
c
c*****Berechnung der Koeffizienten und Ausgabe:
c
        write (6,400)
400   format (6x,'b[grd]',2x,'c[m/s]',3x,'Ma[-]',5x,'Re[-]',
1          5x,'kb[-]',5x,'kg[-]',5x,'kt[-]',5x,'ks[-]')
c
        do 500 i=1, n
            rho=pu/(R*(t(i)+273.15))
            pt=ptpu(i)+pu
            c=sqrt(2*(pt-pu)/rho)
            Ma=c/(sqrt(kappa*R*(t(i)+273.15)))
c
c*****Kinemat. Zaehigkeit von Luft, 0 - 60 grd, 1.0132bar
c
        Dubbel, Seite 1356:
        nu=(0.09401*t(i)+13.24129)*1.0E-6
c*****
c
        Re(i)=c*d/(1000.0*nu)
c
        pq=(p2pu(i)+p3pu(i)+p4pu(i)+p5pu(i)+4*pu)/4.0
c
        kb=(p2pu(i)-p3pu(i))/(p1pu(i)+pu-pq)
c
        kg=(p4pu(i)-p5pu(i))/(p1pu(i)+pu-pq)
c
        kt=(p1pu(i)+pu-pt)/(p1pu(i)+pu-pq)
c

```

```

        ks=(pq-pu)/(p1pu(i)+pu-pq)
c
        write (6,420) dbeta(i), c, Ma, Re(i), kb, kg, kt, ks
420      format (2x,f10.1,f8.2,f8.3,f10.1,4f10.3)
c
500      continue
c
c*****Minimale und maximale Reynoldszahl:
c
        Remin=Re(1)
        do 520 i=1, n
            if (Re(i).lt.Remin) then
                Remin=Re(i)
            endif
520      continue
c
        Remax=Re(1)
        do 530 i=1, n
            if (Re(i).gt.Remax) then
                Remax=Re(i)
            endif
530      continue
c
        write (6,540)
540      format (6x)
        write (6,550) Remin, Remax
550      format (6x,'Re_min=',f6.0,4x,'Re_max=',f6.0)
c
c*****Schliessen des Eingabefiles 'kalib5.dat':
        close (5)
c
c*****Schliessen des Text-Ausgabefiles 'kalib5.out':
        close (6)
c
        end
c
c*****
        subroutine header
c*****Subroutine zur Ausgabe des Headers
c
        character datum*8, zeit*8
c
c
        call date(datum)
        call time(zeit)
c
        write (6,50) datum, zeit
50      format (6x,72('*'),
1         /6x,'* Institut fuer Thermische Turbomaschinen',
2         14x,'Datum: ',a8, ' *',
3         /6x,'* und Energieanlagen',35x,' Zeit: ',a8,' *')
c
        write (6,60)
60      format (6x,'* Auswertung: Kalibrierung 5-Lochsonde',
2         33x,'*')
c
        write (6,70)
70      format (6x,72('*'),/)
c
        return
        end

```

Endnote II

Hole numbering order

The *United Sensor* probes do not follow the frequently used nomenclature for the hole numbering which was also adopted in this Diploma Thesis. In order to simplify the calibration and avoid any kind of confusions, it was preferred to switch the 2 and 3 take off tubes, instead of changing the Lab VIEW 5.0 program and the definitions of the positive and negative yaw angle ($\pm \Delta\beta$)

The adopted numbering order is presented in table 3 and the manufacturing configuration is shown in figure 29

| Adopted Nomenclature | Conical Probe | Prismatic Short Probe | Prismatic Long Probe |
|----------------------|---------------|------------------------------|-----------------------------|
| 1 | 1 | 1 | 1 |
| 2 | 2 | 3 | 3 |
| 3 | 3 | 2 | 2 |
| 4 | 4 | 4 | 4 |
| 5 | 5 | 5 | 5 |

Table 3: Adopted nomenclature

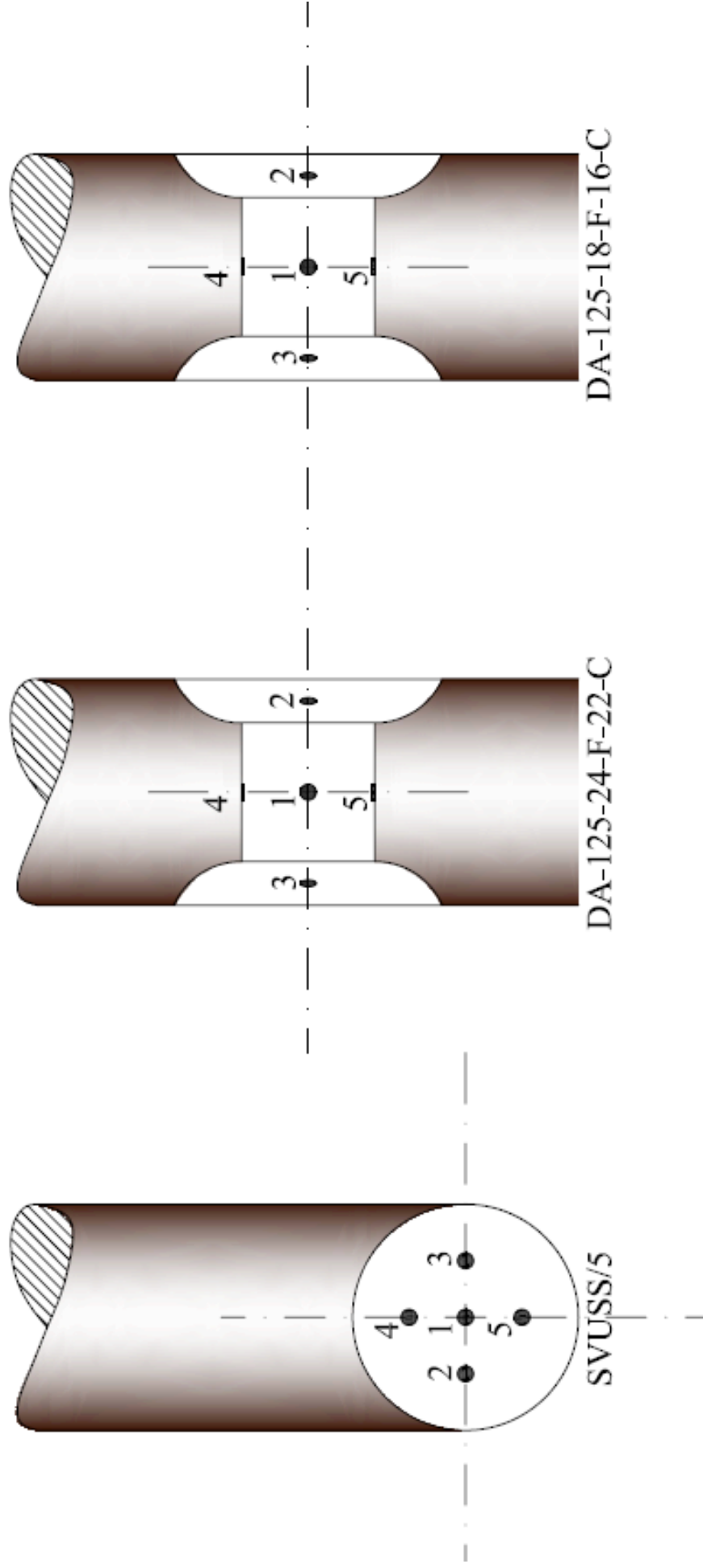


Figure 30: Manufacturing configuration

Bibliography

- [1] **Dominy R.G., Hodson H. P.:** *An Investigation of Factors Influencing the Calibration of Five-Hole Probes for Three-Dimensional Flow Measurements.* ASME Journal of Turbomachinery, Vol. 115 (July 1993)
- [2] **Gieß P. A., Rehder H.J. and Kost. F.:** *A New Test Facility for Probe Calibration – Offering Independent Variation of Mach and Reynolds Number.* Proceedings of the 15th Bi-Annual Symposium on Measuring Techniques in Transonic and Supersonic Flow in Cascades and Turbomachines. Firenze, Italy. (September 2000)
- [3] **Goldstein R. J.:** *Fluid Mechanics Measurements.* Springer-Verlag. Berlin. ISBN 3-540-12501-9 (1976)
- [4] **Lee S.W., Jun S. B.:** *Effects of Reynolds Number on the Non-Nulling Calibration of a Cone-Type Five-Hole Probe.* ASME Paper GT 2003 - 38147 (June 2003)
- [5] **Morrison G.L., Schobeiri M.T., and Pappu K.R.:** *Five-Hole Pressure Probe Analysis Technique.* Flow Measurement and Instrumentation 9 (June 1998)
- [6] **Pisasale A. J., Ahmed N.A.:** *A Novel Method for Extending the Calibration Range of Five-Hole Probe for Highly Three-Dimensional Flows.* Flow Measurement and Instrumentation 13 (March 2002)
- [7] **Sitaram N., Lakshminarayana B., and Ravindranath A.:** *Conventional Probes for the Relative Flow Measurement in a Turbomachinery Rotor Blade Passage.* ASME Journal of Engineering for Power, Vol. 103 (April 1981)
- [8] **Treaster A.L., Yocum, A.M:** *The Calibration and Application of Five-Hole Probes.* ISA Transactions Vol. 18, No.3 (1979)
- [9] **Truckenbrodt, E.:** *Lehrbuch der angewandten Fluidmechanik. 2.Auflage, Springer (1988)*
- [10] **Willinger R., Haselbacher H.:** *A Three-Hole Pressure Probe Exposed to Velocity Gradient Effects – Experimental Calibration and Numerical Investigation.* Conference on Modelling Fluid Flow (CMFF '03). Budapest, Hungary. (September 2003)
- [11] **Wylar J. S.:** *Probe Blockage Effects in Free Jets and Closed Wind Tunnels.* ASME Journal of Engineering for Power, Paper 74-WA/PTC-5 (October 1975)

Picture List

2. Calibration

| | |
|--|---|
| Fig 1: Inviscid flow along a stream tube | 6 |
|--|---|

3. Five-Hole Probes Geometry

| | |
|---|----|
| Figure 2: Adopted geometry nomenclature | 11 |
| Figure 3: Five-hole SVUSS/5 cobra probe | 13 |
| Figure 4: Conical five-hole probe head geometry | 13 |
| Figure 5: SVUSS/5 conical probe head side view | 14 |
| Figure 6: SVUSS/5 conical probe head front view | 14 |
| Figure 7: Sketch for the SVUSS/5 conical probe | 16 |
| Figure 8: United Sensor ordering form | 17 |
| Figure 9: DA-125-18-F-16-C prismatic probe | 18 |
| Figure 10: DA-125-18-F-16-C head front view | 18 |
| Figure 11: DA-125-18-F-16-C head side view | 18 |

4. Streamline Projection Method

| | |
|--|----|
| Figure 12: Flow velocity analysis | 21 |
| Figure 13: Flow velocity components on the yaw plane | 22 |
| Figure 14: Flow velocity components on the pitch plane | 23 |

5. Test Facility

| | |
|---|----|
| Figure 15: Vienna University of Technology free jet wind tunnel | 27 |
| Figure 16: Support device and probe location | 28 |
| Figure 17: Hardware and software connections for the data acquisition | 30 |

6. Results and Discussion

| | |
|--|----|
| Fig.18: Direction coefficient k_β for conical probe | 38 |
| Fig.19: Direction coefficient k_γ for conical probe | 39 |
| Fig.20: Static pressure coefficient k_s for conical probe | 40 |
| Fig.21: Total pressure coefficient k_t for conical probe | 41 |
| Fig.22: Direction coefficient k_β for prismatic long probe | 44 |
| Fig.23: Direction coefficient k_γ for prismatic long probe | 45 |
| Fig.24: Static pressure coefficient k_s for prismatic long probe | 46 |
| Fig.25: Total pressure coefficient k_t for prismatic long probe | 47 |
| Fig.26: Comparison k_β between short-long prismatic probe | 49 |
| Fig.27: Comparison k_γ between short-long prismatic probe | 50 |
| Fig.28: Comparison k_s between short-long prismatic probe | 51 |
| Fig.29: Comparison k_t between short-long prismatic probe | 52 |

Endnote II

| | |
|--|----|
| Figure 30: Manufacturing configuration | 60 |
|--|----|

Table list

5. Test Facility

| | |
|--|----|
| Table 1: Main data of the wind tunnel | 27 |
| Table 2: Calibration at $Re=13.000$ and $Re=6.500$ | 32 |

Endnote II

| | |
|-------------------------------------|----|
| Table 3: Adopted nomenclature | 59 |
|-------------------------------------|----|